Article

A Polymer Prodrug Strategy to Switch from Intravenous to Subcutaneous Cancer Therapy for Irritant/Vesicant Drugs

Alexandre Bordat, Tanguy Boissenot, Nada Ibrahim, Marianne Ferrere, Manon Levêque, Léa Potiron, Stéphanie Denis, Sébastien Garcia-Argote, Olivia Carvalho, Jérôme Abadie, Catherine Cailleau, Grégory Pieters, Nicolas Tsapis,* and Julien Nicolas*

Read Online

ACCESS | Metrics & More | Article Recommendations | SI Supporting Information

ABSTRACT: Chemotherapy is almost exclusively administered via the intravenous (IV) route, which has serious limitations (e.g., patient discomfort, long hospital stays, need for trained staff, high cost, catheter failures, infections). Therefore, the development of effective and less costly chemotherapy that is more comfortable for the patient would revolutionize cancer therapy. While subcutaneous (SC) administration has the potential to meet these criteria, it is extremely restrictive as it cannot be applied to most anticancer drugs, such as irritant or vesicant ones, for local toxicity reasons. Herein, we report a facile, general, and scalable approach for the SC administration of anticancer drugs through the design of well-defined hydrophilic polymer prodrugs. This was applied to the anticancer drug paclitaxel (Ptx) as a worst-case scenario due to its high hydrophobicity and vesicant properties (two factors promoting necrosis at the injection site). After a preliminary screening of well-established polymers used in nanomedicine, polyacrylamide (PAAm) was chosen as a hydrophilic polymer owing to its greater physicochemical, pharmacokinetic, and tumor accumulation properties. A small library of Ptx-based polymer prodrugs was designed by adjusting the nature of the linker (ester, diglycolate, and carbonate) and then evaluated in terms of rheological/viscosity properties in aqueous solutions, drug release kinetics in PBS and in murine plasma, cytotoxicity on two different cancer cell lines, acute local and systemic toxicity, pharmacokinetics and biodistribution, and finally their anticancer efficacy. We demonstrated that Ptx-PAAm polymer prodrugs could be safely injected subcutaneously without inducing local toxicity while outperforming Taxol, the commercial formulation of Ptx, thus opening the door to the safe transposition from IV to SC chemotherapy.
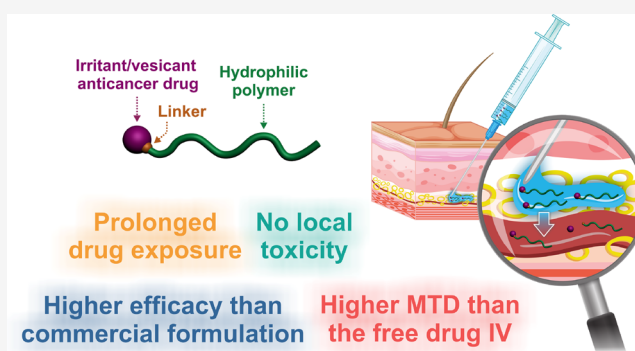
INTRODUCTION

Due to population growth and aging, the number of new cancer cases is expected to increase by approximately 70% over the next 20 years.[1,2] As a result, not only will more and more patients have to deal with cancer, but hospital organization will be strained while patients and health care systems will face an increasing financial burden.[3,4] In addition, since chemotherapy is mostly administered intravenously (IV),[5] it is usually accompanied by severe limitations that are directly responsible for patient discomfort and the high cost of cancer treatments: (i) injectable formulations must be prepared in chemotherapy reconstitution units; (ii) administration must be performed by qualified workers at the hospital, often via a central IV route that requires an implantable chamber; (iii) the patient must stay at the hospital during treatment to be monitored for an early detection of infusion-related toxicities; and (iv) catheter failures and life-threatening infections often occur.[6,7] Therefore, the development of effective chemotherapy that is more comfortable and less dangerous for the patient and also less costly, to significantly decrease the financial burden on patients

and health care systems, represents an urgent and unmet clinical need.

To address this challenge, one can turn to the area of subcutaneous (SC) injectables, which have key advantages over the IV route.[8] SC administration is indeed much more comfortable for the patient than IV administration as it is less invasive and easy to implement.[9] Also, no hospital stay is required, making home chemotherapy and even self-administration possible.[10] Compared to the oral route, SC administration offers superior bioavailability (>80%), faster and better controlled absorption of the drug, drastically reduced compliance problems, and lower variability between patients.[11]
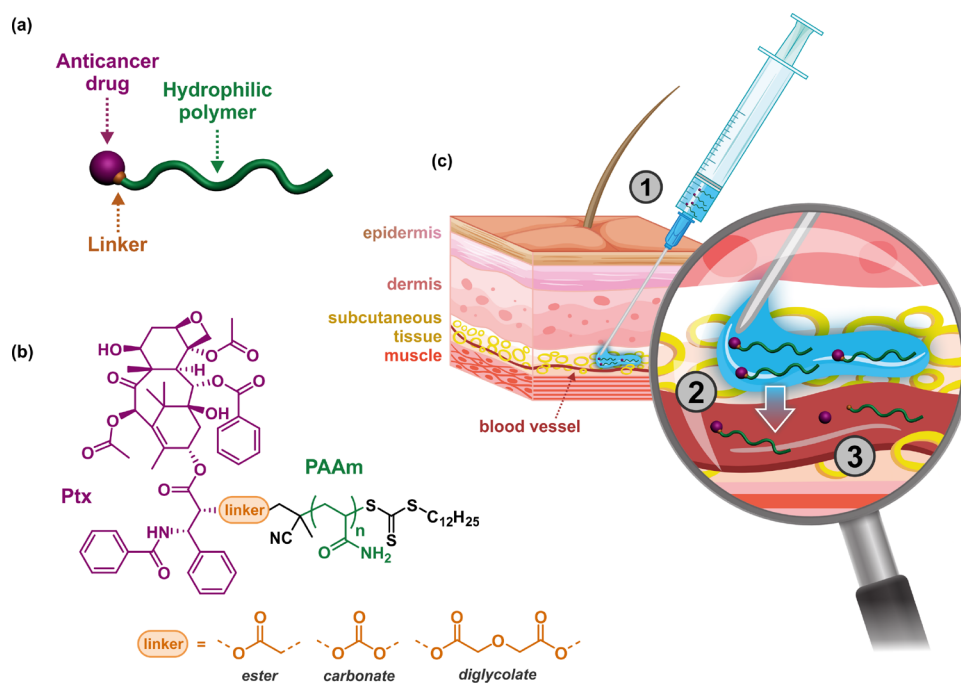
Figure 1. (a) Schematic representation of the water-soluble polymer prodrug used in this work. (b) Chemical structure of paclitaxel-*linker*-polyacrylamide (Ptx-*linker*-PAAm) polymer prodrugs with three different linkers (i.e., ester, carbonate, and diglycolate). (c) Subcutaneous administration of an aqueous solution of Ptx-polymer prodrugs (1) followed by their absorption by the blood/lymph vessels (2) and release of Ptx after linker cleavage (3).

The technologies currently developed for the SC administration of small drugs/therapeutic proteins are mainly based on either their direct administration,[11,12] with strategies to increase their aqueous stability (e.g., cyclodextrins, BioChaperone)[13,14] or SC injection volume (e.g., hyaluronidase),[15,16] or on the injection of drug-loaded nanoscale systems (e.g., hydrogels, nanoparticles, liposomes, lipid prodrugs).[17−19] However, these approaches cannot be applied to the vast majority of anticancer drugs. The field of SC injectables for cancer therapy is indeed extremely restricted[11] because most anticancer drugs (including very effective ones such as taxanes, vinca alkaloids, doxorubicine, etc.) are an irritant or vesicant. They induce prohibitive local toxicity such as severe irritation and necrosis,[20] which are triggered by their prolonged retention in SC tissue due to their high lipophilicity. Anticancer drugs are thus repeatedly internalized by SC cells, causing their death and preventing the healing process.[21−23]

Herein, we report the first preclinical development of a general strategy for the SC administration of irritant/vesicant, anticancer drugs. Our idea is based on the design of water-soluble polymer prodrugs comprising one anticancer drug molecule attached at the extremity of a well-defined, water-soluble polymer chain (Figure 1a). To demonstrate the proof of concept, we chose paclitaxel (Ptx), a representative hydrophobic irritant/vesicant anticancer drug widely used in the clinic. After a preliminary screening of different well-established polymers used in nanomedicine, polyacrylamide (PAAm) was selected owing to its favorable physicochemical, pharmacokinetic, and tumor accumulation properties. PAAm is an uncharged, highly water-soluble, and biocompatible polymer,[24,25] with stealth properties and also employed as a permanent dermal filler (Aquamid).[26] It thus fully meets the criteria for SC administration as recommended by Mrsny and Kinnunen.[27] Ptx was bound to PAAm via a cleavable linker

positioned on its C2′ hydroxyl group,[28] resulting in inactive Ptx-based prodrugs (Figure 1b). The prodrugs' characteristics thus (i) prevent early release of the drug into the SC tissue, (ii) promote their diffusion throughout the SC tissue and absorption into blood/lymph capillaries to yield high bioavailability, and (iii) allow the drug to be released into the bloodstream where it can exert its therapeutic activity (Figure 1c).

We showed that our strategy is safe as no local toxicity was observed. Precise tuning of the prodrug structure also allowed us to greatly decrease the peak drug concentration (C_{max}), responsible for systemic toxicity,[29] while achieving sustained drug exposure. Importantly, our approach enabled a 3-fold increase of the maximum tolerated dose (MTD) and therefore a greater anticancer efficacy when benchmarked against IV-administered Taxol, the most common commercial formulation of Ptx.

■ EXPERIMENTAL SECTION

Materials. Acrylamide (AAm, ≥99%) was purchased from Sigma-Aldrich and recrystallized from chloroform. Azobisisobutyronitrile (AIBN, 98%) was purchased from Sigma-Aldrich and recrystallized from ethanol. Hydroxypropyl methacrylamide (HPMA, 99%), oligo(ethylene glycol)methylether methacrylate (OEGMA, M_n ~ 300 g mol^{-1}), 2-methacryloyloxyethyl phosphorylcholine (MPC, 97%), 4-cyano-4-[(ethylsulfanylthiocarbonyl)sulfanyl]pentanoic acid (95%, CEP), 4-cyano-4-[(dodecylsulfanylthiocarbonyl)sulfanyl]-pentanoic acid (CDSPA, 97%), 4-cyano-4-[(dodecylsulfanylthiocarbonyl)sulfanyl]pentanol (CDP), *N*-hydroxy-succinimide (NHS, 98%), 4-dimethylaminopyridine (≥96.5%, DMAP), 1-(3-dimethylaminopropyl)-3-ethylcarbodiimide hydrochloride (≥98%, EDC·HCl), diglycolic anhydride (≥96.0%), triethylamine (TEA, 99%), RPMI-1640 cell culture medium, insulin from bovine pancreas, Eagle's minimum essential medium (EMEM), and Dulbecco's modified Eagle's medium/nutrient mixture F-12 HAM (DMEM F-12 HAM) were purchased from Sigma-Aldrich and used

as received. Cyanine 5.5 (Cy5.5) was purchased from Lumiprobe and used as received. MeO-PEG-NHS (M_n = 23,000 g mol^{-1}) and MeO-PEG-COOH (M_n = 23,000 g mol^{-1}) were purchased from Iris Biotech and used as received. Paclitaxel (Ptx) was purchased from Carbosynth, [^{3}H]-paclitaxel (3 Ci mmol^{-1}, 1 mCi) was purchased from Moravek, and both were used as received. Ptx-*diglycolate*-CDP was synthesized as described elsewhere.[30] Deuterium oxide (D$_2$O), deuterated chloroform (CDCl$_3$), deuterated Ptx, and deuterated dimethyl sulfoxide (d_6-DMSO) were obtained from Eurisotop. Taxol was purchased from Fresenius Kabi France. All solvents were purchased from Sigma-Aldrich at the highest grade.

Analytical Methods. *Nuclear Magnetic Resonance (NMR) Spectroscopy.* ^{1}H NMR and ^{13}C NMR spectroscopy of small molecules were performed in 5 mm diameter tubes in deuterated chloroform (CDCl$_3$) on a Bruker Avance 300 spectrometer operating at 300 MHz (^{1}H) or 75 MHz (^{13}C) at room temperature. ^{1}H NMR spectroscopy of polymers was performed on a Bruker Avance 3 HD 400 spectrometer operating at 400 MHz in 5 mm diameter tubes: (i) in d_6-DMSO (70 °C, 128 scans) or in D$_2$O (70 °C, 128 scans) for PAAm-based polymers; (ii) in D$_2$O (70 °C, 128 scans) for NHS-PMPC, NHS-PHPMA and NHS-POEGMA polymers; and (iii) in CDCl$_3$ (25 °C, 128 scans) for Ptx-PEG polymer.

Size Exclusion Chromatography (SEC). SEC was performed on a setup from Viscotek (TDAmax) composed of a TDA 305 Triple Detector Array containing a differential viscometer, a right-angle laser-light scattering (90°, RALLS) detector, a low-angle laser-light scattering (7°, LALLS) detector, and a refractive index (RI) detector. The chromatographic column set consisted of a guard column (PL, 50 × 7.5 mm) followed by two columns (PSS Gram, 300 × 8 mm; bead diameter 10 μm; molar mass range 500–10^6 g mol^{-1}). The system was equipped with a triple detection system (Viscotek TDA/GPCmax from Malvern) comprising a differential refractive index detector, low and right-angle light scattering detectors, a differential viscometer detector, and a UV detector. The GPCmax was composed of an on-line degasser and a dual piston pump set at a flow rate of 0.7 mL min^{-1} with DMSO as the eluent, previously filtered through a 0.2 μm filter. The TDAmax was thermostated at 50 °C. The system was calibrated using a narrow pullulan standard, and each polymer sample was injected at 5 different injection volumes to determine the refractive index increment (dn/dc = 0.057 mL g^{-1}). Before the injection (100 μL), the samples were filtered through a polytetra-fluoroethylene (PTFE) membrane with 0.2 μm pores. This allowed the molar mass ($M_{n,SEC}$) and the dispersity ($Đ = M_w/M_n$) of the polymers to be determined by triple detection using the OmniSEC software version 4.6.1.354.

Rheological Measurements. All rheological measurements were carried out on a rotational rheometer ARG2 (TA instruments, New Castle, USA). The geometry was an aluminum plate/plate (diameter 20 mm) equipped with a solvent trap. The TRIOS software was used for data analysis. Flow properties of the prodrugs were determined at 20 °C by a stress sweep. After a 2 min equilibration time, the shear rate was increased gradually from 10 to 1000 s^{-1}.

Injectability. Injectability tests were carried out using a custom-built device described previously.[31] This device was coupled to a texture analyzer TAXT2 (Stable MicroSystems, Godalming, UK) in compression mode, which was equipped with a force transducer calibrated with a 30 kg sensor. 400 μL of solution was taken in a 1 mL syringe (MeritMedical, Medaillon Syringe, USA), which was then fitted with a 26 G × $^1/_2$″ needle (0.45 × 12 mm, Terumo Neolus, Japan) before injection at a 1 mm s^{-1} rate.

Fluorescence Imaging. Fluorescence was monitored using an IVIS Lumina LT series III (PerkinElmer, USA) imaging system. Filters were selected according to the Cyanine 5.5 emission and excitation spectra (640 nm excitation; 695–770 nm emission filter). The imaging signals were analyzed using the Living Image software (PerkinElmer, USA). The tumors were selected as a region of interest (ROI), and the same ROI in the contralateral anatomical region was selected as non-specific background signals. The ratio of the total radiant efficiency of the tumor ROI to the background ROI is calculated and allows comparison of the different polymers by normalizing to the amounts of fluorescence injected.

Liquid Chromatography–Tandem Mass Spectrometry (LC–MS/MS). Liquid chromatography conditions were as follows: C$_{18}$ (HILIC) column (Nucleodur, EC 125/2, 100-5-C18, Macherey-Nagel, Hoerdt, France). Mobile phase: acetonitrile/water (50/50, v/v) with formic acid 0.1%; run time: 8 min; flow rate: 0.3 mL min^{-1}. ESI-MS/MS analyses were performed on a triple quadrupole mass spectrometer detector (TQD) with an electrospray ionization (ESI) interface (Quattro Ultima, Waters, Guyancourt, France). Electrospray and mass parameters were optimized by direct infusion of pure analytes into the system. ESI parameters: capillary voltage of 3.5 kV, cone voltage of 35 V, source temperature of 120 °C, desolvation temperature of 350 °C, with a nitrogen flow of 506 L h^{-1}. Mass parameters: transitions were monitored as follows: Ptx 854/286; Ptx-d$_5$ 859/291. Calibration: calibration curve was linear in the range 5–1000 ng mL^{-1} ($y = 0.0047x + 0.0838$; R^2 = 0.9936 in PBS and y = $0.0052x − 0.0131$; R^2 = 0.9949 in mouse plasma).

Synthesis. *Synthesis of NHS-CEP.* In a 250 mL round-bottom flask, CEP (7.6 mol, 2.0 g) and NHS (9.12 mol, 1.05 g) were dissolved in DCM (150 mL). The mixture was sonicated for 3.5 min in an ultrasonic bath. A solution of DCC (7.61 mmol, 1.572 g) in DCM (40 mL) was added dropwise at 0 °C. The reaction mixture was stirred overnight at room temperature. A white precipitate was observed, which was filtered. The impurities were eliminated by extraction with water. The organic layer was evaporated, and then the crude was triturated with diethyl ether. The product was recrystallized from DCM/cyclohexane (1/1, v/v) to give a yellow powder. Yield = 66%. ^{1}H NMR (300 MHz, CDCl$_3$): δ 3.38 (q, J = 7.4 Hz, 2H), 3.05–2.78 (m, 6H), 2.77–2.45 (m, 2H), 1.93 (s, 3H), 1.40 (t, J = 7.4 Hz, 3H). ^{13}C NMR (75 MHz, CDCl$_3$): δ 216.30, 168.72, 167.00, 118.60, 46.00, 33.70, 33.20, 31.42, 26.84, 25.55, 24.85, 24.75, 12.67. HRMS (M + H)$^+$: 361.0347; found: 361.0350.

Synthesis of NHS-PAAm. In a 25 mL round-bottom flask, AAm (46 mmol, 3.279 g), NHS-CEP (0.165 mmol, 59.3 mg), and AIBN (0.033 mmol, 5.5 mg) were dissolved in DMSO (11.5 mL). The mixture was degassed with argon for 15 min under vigorous stirring before being placed in a 70 °C-preheated oil bath for 24 h under stirring. After the reaction, the polymer was precipitated twice in methanol (MeOH). The polymer was further solubilized in deionized water and placed in a 3.5 kDa Spectra/Por 3 dialysis bag for dialysis against deionized water for 3 days, with dialysis water changed twice per day. The dialysate was then freeze-dried to yield a white yellowish solid (**NHS-PAAm$^{20\ k}$**). Yield = 66%. ^{1}H NMR (400 MHz, D$_2$O): δ 3.45 (CS_2-CH_2-CH$_3$) 2.65–2.05 (CH_2-CH(CONH$_2$)), 2.05–1.41 (CH$_2$-CH(CONH$_2$)), 1.40–1.27 (CS$_2$-CH$_2$-CH_3). $M_{n,NMR}$ (D$_2$O) = 19,800 g mol^{-1} (by using the 2H from CS$_2$-CH_2-CH$_3$ at 3.45 ppm and the methine and methylene protons from AAm). $M_{n,SEC}$ = 30,200 g mol^{-1}, $Đ$ = 1.2.

The same procedure was adapted as follows to target different molar masses: **NHS-PAAm$^{7.0\ k}$** [AAm (13 mmol, 0.924 g), NHS-CEP (0.1 mmol, 34.5 mg), AIBN (0.02 mmol, 3.2 mg), and DMSO (3.25 mL), reaction time: 2 h. $M_{n,NMR}$ = 7000 g mol^{-1}, yield = 70%] and **NHS-PAAm$^{4.2\ k}$** [AAm (13 mmol, 0.924 g), NHS-CEP (0.2 mmol, 71 mg), AIBN (0.04 mmol, 6.5 mg), and DMSO (3.25 mL), reaction time: 2 h. $M_{n,NMR}$ = 4200 g mol^{-1}, yield = 50%].

Synthesis of Cy5.5-PAAm. In a 25 mL round-bottom flask, **NHS-PAAm$^{20\ k}$** (0.025 mmol, 503 mg, 1 equiv) was dissolved in DMSO (7.5 mL). The mixture was then heated until it becomes completely soluble and bubbled with argon for 5 min. In a separate 10 mL vial, Cy5.5 (0.029 mmol, 19.35 mg, 1.2 equiv) and TEA (7.64 μL, 0.055 mmol, 2 equiv) were dissolved in DMSO (3 mL). The resulting solution was then added dropwise to the former one. The mixture was let under magnetic stirring for 24 h at room temperature in the dark and then precipitated in cold MeOH (200 mL). The product was filtered, dissolved in deionized water and placed in a 3.5 kDa Spectra/Por 3 dialysis bag for dialysis against deionized water for 3 days, with dialysis water changed twice per day. The dialysate was then freeze-dried to give a blue powder **Cy5.5-PAAm$^{20\ k}$**. Yield = 25%. The Cy5.5 content was determined to be 1.44 mol % by UV spectroscopy.

The same procedure was adapted as follows to the synthesis of **Cy5.5-PAAm**[7.0 k] [**NHS-PAAm**[7.0 k] (0.01 mmol, 0.150 g) in DMSO (2.5 mL), Cy5.5 (0.018 mmol, 14.0 mg), and TEA (4.5 μL) in DMSO (1 mL). Yield = 95%. Cy5.5 content: 0.05 mol %] and **Cy5.5-PAAm**[4.2 k]: [**NHS-PAAm**[4.2 k] (0.08 mmol, 0.40 g) in DMSO (6.0 mL), Cy5.5 (0.05 mmol, 40.0 mg), and TEA (24 μL) in DMSO (6.2 mL). Yield = 90%. Cy5.5 content: 0.03 mol %].

Synthesis of **NHS-POEGMA**. In a 10 mL vial, AIBN (2.0 mg, 0.012 mmol), CEP-NHS (14.7 mg, 0.041 mmol), and OEGMA (770.2 mg, 0.81 mmol) were dissolved in DMF (1.3 mL). The vial was closed with a rubber septum, and the mixture was degassed under argon bubbling for 15 min followed by magnetic stirring for 24 h at 70 °C. The mixture was then precipitated in cold diethyl ether/petroleum ether (1/1, v/v). The product was filtered, dissolved in deionized water, and placed in a 3.5 kDa Spectra/Por 3 dialysis bag for dialysis against deionized water for 3 days, with dialysis water changed twice per day. The dialysate was then freeze-dried to give a yellowish oil. Yield = 42%. ^{1}H NMR (400 MHz, D$_2$O): δ 4.31−4.03 (COO-CH_2-CH$_2$), 3.89−3.50 (O-CH_2-CH_2-O), 3.42−3.31 (O-CH_3), 2.32−1.68 (CH_2-C(COO)(CH$_3$)), 1.48−0.70 (C(COO)(CH_3)). $M_{n,SEC}$ = 16,040 g mol^{-1}, Đ = 1.47.

Synthesis of **Cy5.5-POEGMA**. In a 25 mL round-bottom flask, **NHS-POEGMA** (215.3 mg, 0.011 mmol, 1 equiv) was dissolved in anhydrous DCM (7 mL) and the mixture was bubbled with argon for 5 min. In a separate 10 mL vial, Cy5.5 (14.4 mg, 0.019 mmol, 1.7 equiv) and TEA (2.9 μL, 0.021 mmol, 2 equiv) were dissolved in anhydrous DCM (3 mL). The resulting solution was then added dropwise to the former one, and the mixture was let under magnetic stirring for 24 h in the dark at room temperature. The mixture was then precipitated in cold diethyl ether/petroleum ether (1/1, v/v). The product was filtered, dissolved in deionized water, and placed in a 3.5 kDa Spectra/Por 3 dialysis bag for dialysis against deionized water for 3 days, with dialysis water changed twice per day. The dialysate was then freeze-dried to give a blue solid. Yield = 42%. The Cy5.5 content was determined to be 0.3 mol % by UV spectroscopy.

Synthesis of **NHS-PMPC**. In a 10 mL vial, AIBN (2.4 mg, 0.015 mmol), CEP-NHS (16.3 mg, 0.045 mmol), and MPC (889.8 mg, 3.01 mmol) were dissolved in MeOH (3 mL). The vial was closed with a rubber septum, and the mixture was degassed under argon bubbling for 15 min followed by magnetic stirring for 24 h at 60 °C. The mixture was then precipitated in cold acetone. The product was filtered, dissolved in deionized water, and placed in a 3.5 kDa Spectra/Por 3 dialysis bag for dialysis against deionized water for 3 days, with dialysis water changed twice per day. The dialysate was then freeze-dried to give a yellowish solid. Yield = 68%. ^{1}H NMR (400 MHz, D$_2$O): δ 4.45−4.20 (O-CH_2-CH$_2$-O, O-CH_2-CH_2-O), 4.20−4.02 (P-O-CH_2-CH$_2$), 3.78−3.62 (P-O-CH_2-CH$_2$), 3.38−3.13 (N(CH$_3$)$_3$), 2.65−2.53 (CO-CH_2-CH$_2$-CO), 2.24−1.78 (CH_2-C(COO)(CH$_3$)), 1.26−0.78 (CH$_2$-C(COO)CH_3). $M_{n,NMR}$ (D$_2$O) = 25,000 g mol^{-1} (by using the NHS protons and the protons from the trimethylammonium group of MPC).

Synthesis of **Cy5.5-PMPC**. In a 25 mL round-bottom flask, **NHS-PMPC** (216.2 mg, 0.011 mmol, 1 equiv) was dissolved in anhydrous DCM (7 mL) and the mixture was bubbled with argon for 5 min. In a separate 10 mL vial, Cy5.5 (10.8 mg, 0.014 mmol, 1.3 equiv) and TEA (2.9 μL, 0.021 mmol, 2 equiv) were dissolved in anhydrous DCM (3 mL). The resulting solution was then added dropwise to the solution of NHS-PMPC, and the mixture was let under magnetic stirring for 24 h in the dark at room temperature. The crude was placed in a 3.5 kDa Spectra/Por 3 dialysis bag for dialysis in the dark against deionized water for 3 days, with dialysis water changed twice per day. The dialysate was then freeze-dried to give a blue solid. Yield = 75%. The Cy5.5 content was determined to be 0.05 mol % by UV spectroscopy.

Synthesis of **NHS-PHPMA**. In a 10 mL vial, AIBN (1.17 mg, 0.007 mmol), CEP-NHS (12.87 mg, 0.0358 mmol), and HPMA (715 mg, 4.99 mmol) were dissolved in DMF (1.67 mL). The vial was closed with a rubber septum, and the mixture was degassed under argon bubbling for 15 min followed by magnetic stirring for 24 h at 60 °C. The mixture was then precipitated in cold acetone. The product was

filtered, dissolved in deionized water, and placed in a 3.5 kDa Spectra/Por 3 dialysis bag for dialysis against deionized water for 3 days, with dialysis water changed twice per day. The dialysate was then freeze-dried to give a yellowish solid. Yield = 67%. ^{1}H NMR (400 MHz, D$_2$O): δ 4.10−3.85 (CH(CH$_3$)(OH)), 3.40−3.00 (NH-CH_2), 2.20−1.70 (CH_2-C(CONH)(CH$_3$)), 1.30−0.90 (C(OH)CH$_3$, C(CONH)-CH_3). $M_{n,SEC}$ = 15,530 g mol^{-1}, Đ = 1.57.

Synthesis of **Cy5.5-PHPMA**. In a 10 mL vial, **NHS-PHPMA** (202.5 mg, 0.011 mmol, 1 equiv) is dissolved in DMSO (3 mL) and the mixture was bubbled with argon for 5 min. In a separate 10 mL vial, Cy5.5 (9.05 mg, 0.014 mmol, 1.3 equiv) and TEA (2.7 μL, 0.021 mmol, 2 equiv) were dissolved in DMSO (1 mL). The resulting solution was then added dropwise to the former one, and the mixture was let under magnetic stirring for 24 h in the dark at room temperature. The crude was dissolved in deionized water (30 mL) placed in a 3.5 kDa Spectra/Por 3 dialysis bag for dialysis in the dark against deionized water for 3 days, with dialysis water changed twice per day. The dialysate was then freeze-dried to give a blue solid. Yield = 63%. The Cy5.5 content was determined to be 0.25% by UV spectroscopy.

Synthesis of **Cy5.5-PEG**. MeO-PEG-NHS (200 mg, 0.0087 mmol, 1 equiv) was dissolved in DCM (2.5 mL), and the mixture was bubbled with argon for 5 min. In a separate 10 mL vial, Cy5.5 (9.05 mg, 0.014 mmol, 1.12 equiv) and TEA (2.77 μL, 2 equiv) were dissolved in DMSO (1 mL). The resulting solution was then added dropwise to the former one, and the mixture was let under magnetic stirring for 24 h in the dark at room temperature. DCM was evaporated by rotary evaporation, and the product was dissolved in water. The solution was then placed in a 3.5 kDa Spectra/Por 3 dialysis bag for dialysis in the dark against deionized water for 3 days, with dialysis water changed twice per day. The dialysate was then freeze-dried to give a blue solid. Yield = 94%. The Cy5.5 content was determined to be 0.26% by UV spectroscopy.

Synthesis of **Ptx-Ester-CDSPA and [^{3}H]-Ptx-Ester-CDSPA**. CDSPA (121 mg, 0.30 mmol), DMAP (40 mg, 0.33 mmol), and EDC·HCl (67 mg, 0.35 mmol) were dissolved in 2 mL of anhydrous CH$_2$Cl$_2$ and mixed in a reaction flask under argon at room temperature. After 15 min, a solution of Ptx (100 mg, 0.12 mmol) in DMF (0.5 mL) was added dropwise into the flask. After stirring at 30 °C for 4 h, an additional 20 mg (0.10 mmol) of EDC·HCl solution in 200 μL of anhydrous DCM was added. The reaction was stirred at 30 °C for another 22 h and was poured into 20 mL of ethyl acetate (EtOAc). The organic phase was washed with aqueous NaHCO$_3$ and brine before being dried over MgSO$_4$. The residue was concentrated under reduced pressure and purified by flash chromatography (SiO$_2$, from DCM/EtOAc = 5/1 to DCM/EtOAc = 4/1, v/v) to give 88 mg (0.071 mmol) of Ptx-*ester*-CDSPA as a yellow, sticky solid. Yield = 61%. ^{1}H NMR (300 MHz, CDCl$_3$): δ = 8.17 (d, J = 7.6 Hz, 2H), 7.78 (d, J = 7.5 Hz, 2H), 7.72−7.31 (m, 15H), 6.93 (d, J = 8.9 Hz, 1H), 6.54−6.15 (m, 2H), 6.01 (d, J = 8.9 Hz, 1H), 5.70 (d, J = 7.0 Hz, 1H), 5.51 (d, J = 3.2 Hz, 1H), 5.00 (d, J = 8.7 Hz, 1H), 4.47 (s, 1H), 4.28 (dd, J = 34.7, 8.5 Hz, 2H), 3.84 (d, J = 6.8 Hz, 1H), 3.34 (t, J = 9.4 Hz, 1H), 2.51 (d, J = 13.8 Hz, 6H), 2.25 (s, 3H), 1.96 (s, 2H), 1.83 (d, J = 3.1 Hz, 3H), 1.78−1.60 (m, 10H), 1.38−1.13 (m, 20H), 0.90 (t, J = 6.5 Hz, 3H). ^{13}C NMR (75 MHz, CDCl$_3$): δ = 216.8, 203.8, 171.2, 170.7, 169.8, 167.9, 167.0, 142.6, 136.8, 133.7, 133.5, 132.9, 132.0, 130.2, 129.2, 128.7, 128.6, 127.2, 126.5, 119.0, 84.5, 81.1, 79.1, 76.4, 75.6, 75.1, 74.7, 72.1, 72.0, 58.5, 52.8, 46.3, 45.6, 43.2, 37.1, 35.5, 33.6, 31.9, 29.6, 29.5, 29.4, 29.3, 29.1, 28.9, 27.7, 26.8, 24.8, 24.8, 22.7, 22.7, 22.1, 20.8, 14.8, 14.1, 9.6.

For [^{3}H]-Ptx-*ester*-CDSPA, the procedure was the same except that [^{3}H]-Ptx was added into the reaction mixture as follows. Ethanol was carefully evaporated under vacuum from the initial stock solution of [^{3}H]-Ptx. [^{3}H]-Ptx (1 mCi) was then solubilized in 100 μL of DMF prior to addition to the reaction mixture containing non-radiolabeled Ptx (100 mg, 0.12 mmol) and the other reagents in 200 μL of DMF. The vial containing the initial [^{3}H]-Ptx was further rinsed twice with 100 μL of DMF, and these volumes were added to the reaction mixture. The following steps were identical to those described for the synthesis of Ptx-*ester*-CDSPA, and a mixture of Ptx-*ester*-CDSPA/

Table 1. Macromolecular Characteristics and Solubility of the Different Ptx-PAAm Polymer Prodrugs Synthesized in This Study

sample	linker	$M_{n,NMR}$[a] (g mol^{-1})	$M_{n,SEC}$[b] (g mol^{-1})	Đ[b]	%Ptx[c] (wt %)	solubility[d]
P1e	ester	6200	9100	1.07	13.8	insoluble
P2e	ester	9400	15,200	1.28	9.1	insoluble
P3e	ester	21,600	29,100	1.12	4.0	soluble
P3d	digly	27,300	36,000	1.10	3.1	soluble
P3c	carbonate	23,000	39,900	1.09	3.7	soluble

[a]Determined by comparing the integration of the doublet at 8 ppm, corresponding to 2 aromatic protons from one of the Ptx aromatic groups (noted 3 and 7 in Figure S6), and the broad peak at 1.80−1.29 ppm corresponding to methylene protons of AAm. [b]Determined by triple detection SEC. [c]Calculated by $M_{n,NMR}$. [d]Solubility tests were performed in water at a Ptx equivalent concentration of 3 mg mL^{-1} to assess the presence of insoluble aggregates or not.

[^{3}H]-Ptx-*ester*-CDSPA with a total activity of 258 μCi was obtained as a yellow sticky solid. Yield = 19%.

Synthesis of Ptx-Carbonate-CDP. To a solution of Ptx (194 mg, 0.227 mmol) in dry DCM (4 mL) under an argon atmosphere were added 4 drops of pyridine. Then, 4-nitrophenyl chloroformate (273 mg, 1.362 mmol) in dry DCM was added at −50 °C, the reaction mixture was stirred at −50 °C, and after 4 h, 4-nitrophenyl chloroformate (183 mg, 0.908 mmol) was added again. After 1 h, the mixture was diluted with DCM, washed with sodium bicarbonate (NaHCO$_3$, 0.5 N) and brine, and dried over anhydrous sodium sulfate. The organic layer was separated and evaporated under vacuum. After evaporation of the solvents, the crude was purified by column chromatography (ethyl acetate/cyclohexane, 1:1, v/v), to yield activated paclitaxel. Yield = 45%. ^{1}H NMR (300 MHz, CDCl$_3$): δ = 8.28 (d, J = 9.2 Hz, 2H), 8.18 (d, J = 7.2 Hz, 2H), 7.77 (d, J = 7.3 Hz, 2H), 7.69−7.32 (m, 13H), 6.91 (d, J = 9.4 Hz, 1H), 6.33 (d, J = 15.5 Hz, 2H), 6.12 (d, J = 9.5 Hz, 1H), 5.72 (d, J = 7.0 Hz, 1H), 5.55 (d, J = 2.6 Hz, 1H), 4.99 (d, J = 8.0 Hz, 1H), 4.54−4.40 (m, 1H), 4.35 (d, J = 8.3 Hz, 1H), 4.23 (d, J = 8.4 Hz, 1H), 3.84 (d, J = 7.0 Hz, 1H), 2.55−2.40 (m, 4H), 2.34−2.17 (m, 4H), 1.95 (s, 3H), 1.89 (d, J = 16.7 Hz, 1H), 1.81 (s, 1H), 1.71 (s, 3H), 1.67 (s, 2H), 1.28 (s, 3H), 1.17 (s, 3H). ^{13}C NMR (75 MHz, CDCl$_3$): δ = 203.7, 171.2, 169.8, 167.3, 167.1, 154.9, 151.7, 142.3, 136.3, 133.7, 133.3, 133.1, 132.2, 130.2, 129.3, 129.2, 128.8, 128.8, 127.1, 126.5, 125.4, 121.6, 84.4, 81.2, 79.2, 75.5, 72.5, 72.1, 58.5, 52.6, 45.6, 43.2, 35.6, 26.9, 22.8, 22.2, 20.8, 14.8, 9.6.

Activated Ptx (220 mg, 0.215 mmol) and CDP (83 mg, 0.215 mmol) in dry DCM (12 mL) were reacted at room temperature with DMAP (31 mg, 0.258 mmol). The reaction mixture was stirred in the dark for 48 h and was then diluted with DCM. The organic layer was washed with saturated NaHCO$_3$ and dried over anhydrous sodium sulfate. The organic layers were concentrated, and the crude was purified with column chromatography using cyclohexane/ethyl acetate as the eluant (using a gradient from 80/20 to 50/50). The compound was isolated as a yellow powder. Yield 74%. ^{1}H NMR (300 MHz, CDCl$_3$): δ = 8.17 (d, J = 7.3 Hz, 2H), 7.78 (d, J = 8.0 Hz, 2H), 7.68−7.34 (m, 11H), 6.95 (d, J = 9.1 Hz, 1H), 6.32 (s, 2H), 6.02 (d, J = 8.5 Hz, 1H), 5.71 (d, J = 7.1 Hz, 1H), 5.44 (s, 1H), 5.00 (d, J = 8.7 Hz, 1H), 4.55−4.41 (m, 1H), 4.35 (d, J = 8.6 Hz, 1H), 4.23 (d, J = 7.2 Hz, 3H), 3.84 (d, J = 7.5 Hz, 1H), 3.34 (t, J = 7.3 Hz, 2H), 2.58−2.37 (m, 5H), 2.22 (d, J = 19.3 Hz, 5H), 1.96 (s, 4H), 1.89 (s, 3H), 1.71 (s, 8 H), 1.48−1.12 (m, 26H), 0.90 (t, J = 6.5 Hz, 3H). ^{13}C NMR (75 MHz, CDCl$_3$): δ = 203.8, 171.2, 169.9, 167.7, 167.0, 154.0, 142.6, 136.7, 133.7, 132.1, 130.2, 129.2, 128.7, 128.6, 127.2, 126.6, 84.5, 81.1, 79.2, 75.6, 75.1, 72.1, 67.8, 58.5, 57.7, 52.7, 47.2, 46.6, 45.6, 43.2, 37.1, 35.6, 29.6, 28.9, 27.7, 26.9, 24.9, 24.2, 22.7, 22.7, 22.2, 20.8, 14.8, 14.1. MS (ESI)$^+$: 1291.7 (M+ Na)$^+$.

Synthesis of Ptx-Ester-PAAm, Ptx-Diglycolate-PAAm and Ptx-Carbonate-PAAm. To a 7 mL glass vial were added AIBN (0.8 mg, 0.005 mmol), the Ptx-functionalized RAFT agents [Ptx-*ester*-CDSPA (30 mg, 0.024 mmol, for **P3e**), Ptx-*diglycolate*-CDP (30.18 mg, 0.022 mmol, for **P3d**), or Ptx-*carbonate*-CDP (30.18 mg, 0.024 mmol, for **P3c**)], AAm (454 mg, 6.39 mmol), and DMSO (1.6 mL). The mixture was degassed with argon for 15 min under vigorous stirring before being placed in a 70 °C-preheated oil bath for 24 h under

stirring. After the reaction, the polymer was precipitated twice in MeOH. The polymer was further solubilized in DMSO and placed in a 3.5 kDa Spectra/Por 3 dialysis bag for dialysis against deionized water for 3 days, with dialysis water changed twice per day. The dialysate was then freeze-dried to yield Ptx-*ester*-PAAm (**P3e**), Ptx-*diglycolate*-PAAm (**P3d**), or Ptx-*carbonate*-PAAm (**P3c**) as a white-to-yellow, spongy solid. Another two polymerizations were carried out with [AAm]$_0$/[PTX-ester-CDP]$_0$ = 53 (**P1e**) and 123 (**P2e**).

Synthesis of [^{3}H]-Ptx-Ester-PAAm. The radiolabeled [^{3}H]-Ptx-*ester*-PAAm was obtained following the same procedure as for **P3e** except that the previously synthesized mixture of Ptx-*ester*-CDSPA/[^{3}H]-Ptx-*ester*-CDSPA was used as the RAFT agent and the purification only consisted in two precipitations in MeOH. The obtained polymer was thoroughly dried under vacuum before being dissolved directly in PBS. This solution was then mixed with a solution of non-radiolabeled Ptx-*ester*-PAAm **P3e** in PBS to the desired Ptx equivalent concentration and radioactivity for further in vivo studies.

Multigram-Scale Synthesis of Ptx-Ester-PAAm. Synthesis was performed as described previously with some modifications. Briefly, in a round-bottom flask, CDSPA* (3.86 g, 0.0095 mol), DMAP* (0.84 g, 0.0068 mol), and EDC·HCl* (1.78 g, 0.0093 mol) were dissolved in 20 mL of anhydrous CH$_2$Cl$_2$ and 15 drops of anhydrous DMF (*these reagents were added portionwise over 20 h) and mixed in a reaction flask under argon at room temperature. After 15 min, a solution of Ptx (4 g, 0.0046 mol) in DCM (20 mL) was added dropwise into the flask. After stirring at 30 °C for 29 h, the organic phase was washed with aqueous NaHCO$_3$ and brine before being dried over MgSO$_4$. The residue was concentrated under reduced pressure and purified by flash chromatography (SiO$_2$, from DCM/ EtOAc, 8/2, v/v) to give Ptx-*ester*-CDSPA as a yellow solid. Yield = 85%. Into a 250 mL round-bottom flask were added AIBN (36 mg, 0.2 mmol), Ptx-*ester*-CDSPA (1.363 g, 1.089 mmol), AAm (2.613 g, 290 mmol), and DMSO (72.5 mL). The mixture was degassed with argon for 15 min under vigorous stirring before being placed in a 70 °C oil bath for 3 h under stirring. After the reaction, the polymer was precipitated twice in MeOH. The polymer was further solubilized in DMSO and placed in a 3.5 kDa Spectra/Por 3 dialysis bag for dialysis against deionized water for 5 days, with dialysis water changed twice per day. The dialysate was then freeze-dried to yield 14 g of Ptx-*ester*-PAAm ($M_{n,NMR}$ = 24,000 g mol^{-1}, $M_{n,SEC}$ = 24,780 g mol^{-1}, Đ = 1.17) as a white-to-yellow spongy solid. Yield = 70%.

Determination of Residual Acrylamide. Analyses were achieved by HPLC via isocratic runs (phosphate buffer mobile phase, 0.6 mL min^{-1} flow rate) on a RP-C18 column (5 μm particle size, 250 × 4.6 mm) and a guard column (5 × 3.9 mm) at a wavelength detection of 208 nm and temperature of 40 °C. Run time was 10 min. Isocratic analyses were performed with a phosphate buffer mobile phase (0.84 g of KH$_2$PO$_4$ in 960 mL of H$_2$O and 40 mL of MeOH). Concentrations of 0.1, 0.5, 1, 2, 10, 30, 50, and 100 μg mL^{-1} AAm in deionized water were used to build the calibration curve. Each concentration was injected 4 times. Samples from **P3e** at 25, 50, and 100 mg mL^{-1} in deionized water were used to determine the residual amount of AAm. Column washing between each run was performed by 1 wash with distilled-deionized water and 1 wash with MeOH.

Synthesis of Ptx-PEG. MeO-PEG-COOH (1.0 g, 0.043 mmol) was dissolved in anhydrous DCM (20 mL). The resulting solution was cooled down to 0 °C before addition of DCC (64 mg, 0.3 mmol), Ptx (252 mg, 0.3 mmol), and DMAP (65 mg, 0.3 mmol). The reaction medium was slowly warmed to room temperature and allowed to stand overnight under stirring before being washed with 0.1 N HCl. The organic layer was dried over $MgSO_4$, filtered through fritted glass, and evaporated under vacuum to yield the product as a white solid. It was then solubilized in deionized water and placed in a 3.5 kDa Spectra/Por 3 dialysis bag against deionized water for 2 days, with dialysis water changed twice per day. The dialysate was then freeze-dried to give a white powder. Coupling yield = 97% (determined by ^1H NMR in $CDCl_3$). Overall yield = 70%.

In Vitro Evaluation. *Drug Release.* Ptx release experiments were performed in PBS (1×, pH 7.4 with 1 wt % Tween 80) and in mouse plasma. Free Ptx, **P3e**, **P3d**, and **P3c** (Table 1) were incubated in PBS and plasma at 37 °C at the same concentration in Ptx (1 μg mL^{-1} equiv Ptx). 200 μL samples was taken at 0, 2, 4, 6, 24, and 48 h, for quantification. The samples were mixed with 600 μL of acetonitrile and 20 μL of a solution of deuterated Ptx (Ptx-d_5) at 1 μg mL^{-1} (internal standard). Samples were shaken for 15 min and centrifuged at 3000 × g for 10 min before analysis by LC–MS/MS.

Cell Culture and Cytotoxicity. The cytotoxicity of the different prodrugs was evaluated on two human breast cancer cell lines (MCF-7 and SK-BR-3), obtained from ATCC (USA). SK-BR-3 cells were cultured in DMEM F-12 HAM supplemented with penicillin (50 U mL^{-1}), streptomycin (50 μg mL^{-1}), 20% heat inactivated FBS, and 0.01 mg mL^{-1} bovine insulin. MCF-7 cells were grown in EMEM supplemented with penicillin (50 U mL^{-1}), streptomycin (50 μg mL^{-1}), 10% heat-inactivated FBS, 1% non-essential amino acids (NEAA), and 5 mL of glutamine. Both types of cells were maintained at 37 °C and 5% CO_2 in a humidified atmosphere and were split twice weekly. The cell viability was evaluated using the 3-[4,5-dimethylthiazol-2-yl]-3,5-diphenyltetrazolium bromide (MTT) assay. Cells were seeded in 100 μL of culture medium (8 × 10^3 cells/well for SK-BR-3 cells and 5 × 10^3 cells/well for MCF-7 cells) in 96 well plates (TPP, Switzerland) and pre-incubated for 24 h. 100 μL of a serial dilution of prodrug solution was then added to the medium. After 72 h of incubation, 20 μL of MTT solution (5 mg mL^{-1} in PBS) was added to each well. After 4 h of incubation, the culture medium was gently aspirated and replaced by 200 μL of DMSO to dissolve the formazan crystals. The absorbance of the solubilized dye, which correlates with the number of living cells, was measured with a microplate reader (LAB Systems Original Multiscan MS, Finland) at 570 nm. The percentage of viable cells in each well was calculated as the absorbance ratio between prodrug-treated and untreated control cells. Data was fitted to a Hill slope model with four parameters using GraphPad Prism (version 8.0.2) to determine the IC$_{50}$. The different IC$_{50}$ values were determined using a one-way ANOVA test with GraphPad Prism (version 8.0.2).

In Vivo Evaluation. *Ethic Protocols.* All animal experiments were conducted according to the European rules (86/609/EEC and 2010/63/EU) and the Principles of Laboratory Animal Care and legislation in force in France (Decree No. 2013-118 as of February 1, 2013). Toxicity, pharmacokinetics, and biodistribution experiments obtained experimental approval from the Ethical Committee C2EA-26 (Comité d'éthique en expérimentation animale de l'IRCIV, Authorization number APAFIS#7756). In vivo efficacy experiments were performed by Oncodesign (Les Ulis, France) as study N°190015 and was approved by the Institutional Animal Care and Use Committee of Oncodesign (Oncomet) approved by French authorities (CNREEA agreement N° 91).
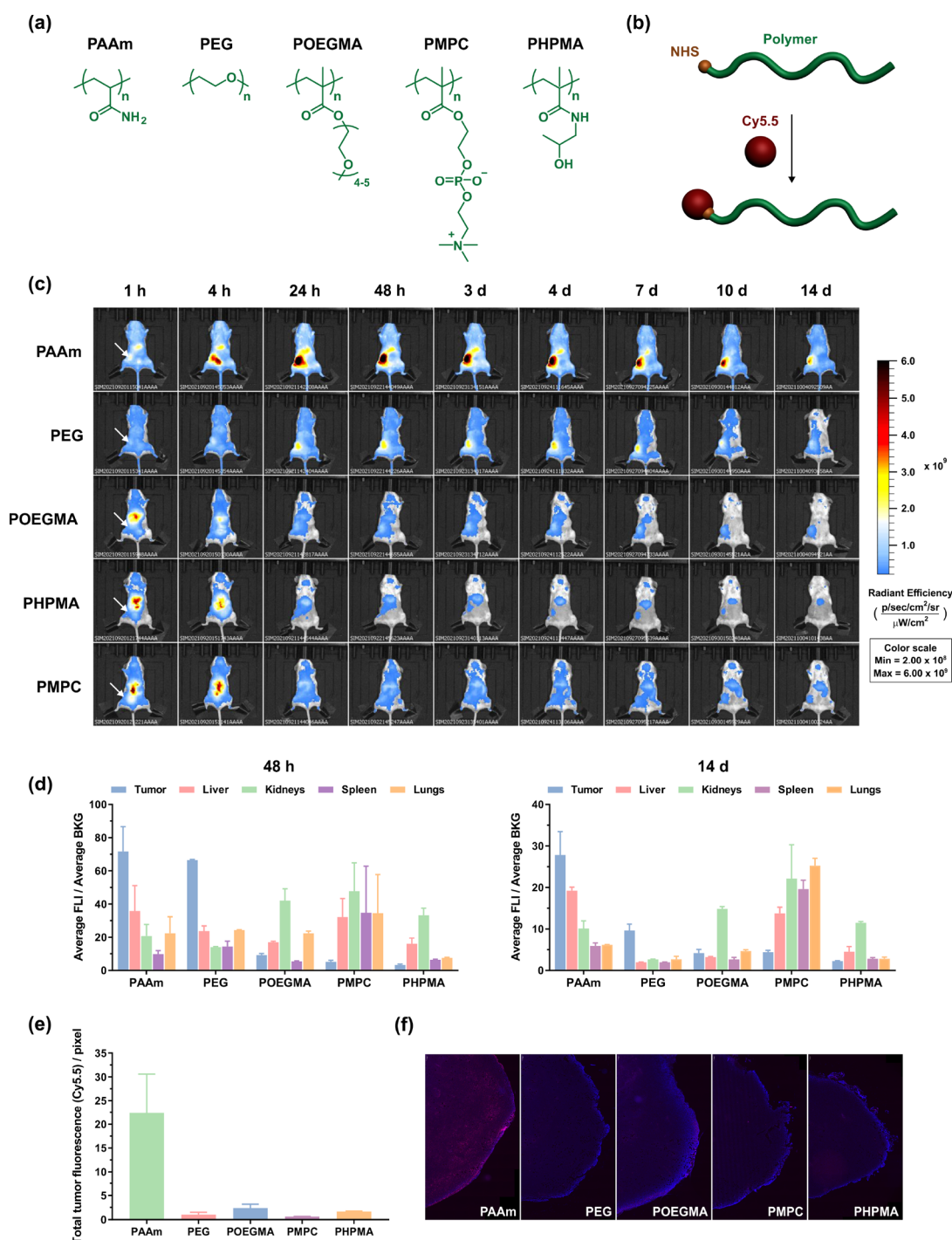
Preliminary Screening of Different Water-Soluble Polymers. 4T-1 murine breast cancer cells were harvested using trypsin, centrifuged at 200g for 5 min at 4 °C then washed with PBS. Cells were resuspended in PBS to obtain a final concentration of 2 × 10^7 cells mL^{-1}. For tumor implantation, mice were anesthetized with 3% isoflurane and laid on their back, their skin was cleaned with betadine, and a 5 to 10 mm incision in the skin was performed so the mammary fat pad could be seen. 50 μL of cell suspension corresponding to 1 ×

10^6 cells was then injected carefully into the mammary fat pad, after which the incision was sutured, and the mouse was monitored until recovery from anesthesia. Tumor volume was measured twice a week with a caliper and estimated with the following formula: volume = (length × width^2)/2 until day 11 where the tumors measured on average 265 ± 55 mm^3. At this time, mice were randomly divided into 13 groups of 2 mice as follows: (i) groups 1−5: **Cy5.5-PAAm$^{20\ k}$**, **Cy5.5-PHPMA**, **Cy5.5-POEGMA**, **Cy5.5-PMPC**, and **Cy5.5-PEG**. Retro-orbital injection (100 μL, 35 mg mL^{-1}) was performed at day 0, and fluorescence imaging was performed at different time points (1 h, 4 h, day 1, day 2, day 3, day 4, day 7, day 10, and day 14). At day 14, mice were sacrificed. Organs and tumor were collected and imaged for fluorescence. (ii) Groups 6−10: **Cy5.5-PAAm$^{20\ k}$**, **Cy5.5-PHPMA**, **Cy5.5-POEGMA**, **Cy5.5-PMPC**, and **Cy5.5-PEG**. Retro-orbital injection (100 μL, 35 mg mL^{-1}) was performed at day 0. At day 2, mice were sacrificed. Organs and tumor were collected and imaged for fluorescence. (iii) Groups 11−13: **Cy5.5-PAAm$^{4.2\ k}$**, **Cy5.5-PAAm$^{7.0\ k}$** and **Cy5.5-PAAm$^{20\ k}$**. Retro-orbital injection (100 μL, 35 mg mL^{-1}) was performed at day 0, and fluorescence imaging was performed at day 1 and day 2. At day 2, the mice were sacrificed. Organs and tumor were collected and imaged for fluorescence. After imaging, all the tumors were fixed in PFA 4%. They were then transfer in 70% ethanol for a maximum of 1 week before paraffin embedding (System Logos One, Micro France). After paraffin embedding, 4 μm-thick tissue sections were made using a microtome (Autosection, Sakura). The slides were then stained (Austostainer XL, Leica) with DAPI (4′,6-diamidino-2-phenylindole) before histopathological examination.

Acute Toxicity and Histology. Groups of 3 mice were injected subcutaneously at day 0 in the interscapular region. The different groups are as follows: (i) Taxol at 60 and 90 mg kg^{-1} (positive control); (ii) PAAm at 700, 1400, 2100, 2800, 3500, and 4200 mg kg^{-1} (polymer alone, negative control); (iii) Ptx-*ester*-PAAm **P3e** at 90, 120, 150, and 180 mg kg^{-1} equiv Ptx; (iv) Ptx-*carbonate*-PAAm **P3c** at 90, 120, 150, and 180 mg kg^{-1} equiv Ptx; and (v) Ptx-*diglycolate*-PAAm **P3d** at 90, 120, 150, and 180 mg kg^{-1} equiv Ptx. Taxol was also injected intravenously in the tail vain at 10, 20, 30, and 60 mg kg^{-1}. Visual toxicities at the injection site and body weight were monitored daily to follow local and systemic toxicities. After 7 days, mice were euthanized by cervical dislocation and injection sites were removed and fixed in PFA 4% (overnight). They were then transfer in 70% ethanol for a maximum of 1 week before paraffin embedding (System Logos One, Micro France). After paraffin embedding, 4 μm-thick tissue sections were made using a microtome (Autosection, Sakura). The slides were then stained (Austostainer XL, Leica) with HES for histopathological examination. A semi-quantitative scoring system, ranging from 0 (no change) to 3 (marked change), was applied.

Pharmacokinetics of Ptx by Mass Spectrometry. Seven week-old female BALB/c OlaHsd mice (~22 g; Envigo, France) were randomly divided into four different groups: (i) Taxol injected intravenously (7 mg kg^{-1}); (ii) Ptx-*ester*-PAAm injected subcutaneously (7 mg kg^{-1} equiv Ptx); (iii) Ptx-*diglycolate*-PAAm injected subcutaneously (7 mg kg^{-1} equiv Ptx); and (iv) Ptx-*carbonate*-PAAm injected subcutaneously (7 mg kg^{-1} equiv Ptx). Each group was composed of 36 mice divided into 9 different time points (0.25, 0.5, 1, 2, 4, 7, 24, 48, and 72 h) leading to 4 mice per group. At each endpoint, mice were euthanized with pentobarbital and blood was sampled by cardiac puncture before plasma was recovered by centrifugation (5 min; 3000 × g). After centrifugation, samples were prepared following the protocol bellow. Aliquots of 200 μL were mixed with 600 μL of acetonitrile and 20 μL of Ptx-d_5 at 1 μg mL^{-1} (internal standard). Samples were shaken for 15 min and centrifuged for 10 min before analysis by LC–MS/MS.

Pharmacokinetics and Biodistribution of Radiolabeled Ptx. Seven week-old female BALB/cOlaHsd mice (~22 g; Envigo, France) were used. Radiolabeled Taxol and radiolabeled [^{3}H]-Ptx-*ester*-PAAm were injected at 7 mg kg^{-1} equiv Ptx (0.93 μCi per mouse) to analyze the pharmacokinetics and the biodistribution. Mice were randomly divided into four groups: (i) Taxol injected

Figure 2. (a) Chemical structures of the water-soluble polymers (PAAm, PEG, POEGMA, PMPC, and PHPMA) investigated during the preliminary screening. (b) Schematic representation of the synthesis of Cyanine 5.5 (Cy5.5)-labeled polymers. (c) Representative in vivo images of fluorescence (λ_{ex} = 640 nm; λ_{em} = 695−770 nm) at different time points of tumor-bearing mice after SC administration (100 μL, 35 mg mL^{-1}) of Cy5.5-labeled polymers. The white arrows indicate the localization of the tumor, and the color bar indicates the total fluorescence radiant efficiency (photons s^{-1} cm^{-2} steradian^{-1} per μW cm^{-2}). (d) Biodistribution obtained by ex vivo fluorescence imaging of different organs (liver, kidneys, spleen, lungs, and tumor) harvested from euthanized tumor-bearing mice after 48 h and 14 days post-SC administration of Cy5.5-labeled polymers (see Figure S1). (e) Total tumor fluorescence (Cy5.5) obtained by ex vivo fluorescence imaging of tumors sections at day 14. (f) Representative ex vivo fluorescence imaging of tumor sections at day 14.

intravenously; (ii) Taxol injected subcutaneously; (iii) [³H]-Ptx-*ester*-PAAm injected intravenously; and (iv) [³H]-Ptx-*ester*-PAAm injected subcutaneously. Each group was composed of 40 mice divided into 10 different time points (0.25, 0.5, 1, 2, 4, 7, 24, 48, 96, and 144 h) leading to 4 mice per group. At each endpoint, mice were euthanized with pentobarbital and blood was sampled by cardiac puncture before

plasma was recovered by centrifugation (5 min at 3000 × g). Livers, kidneys, spleens, lungs, and some SC tissue at the injection site were also collected. All samples were stored in a freezer (−20 °C) before analysis. For radioactivity counting, approximately 100 μL of plasma and 100 mg of each organ/tissue were taken and precisely weighed. Organs were first dissolved by adding 1 mL of solvable (PerkinElmer,
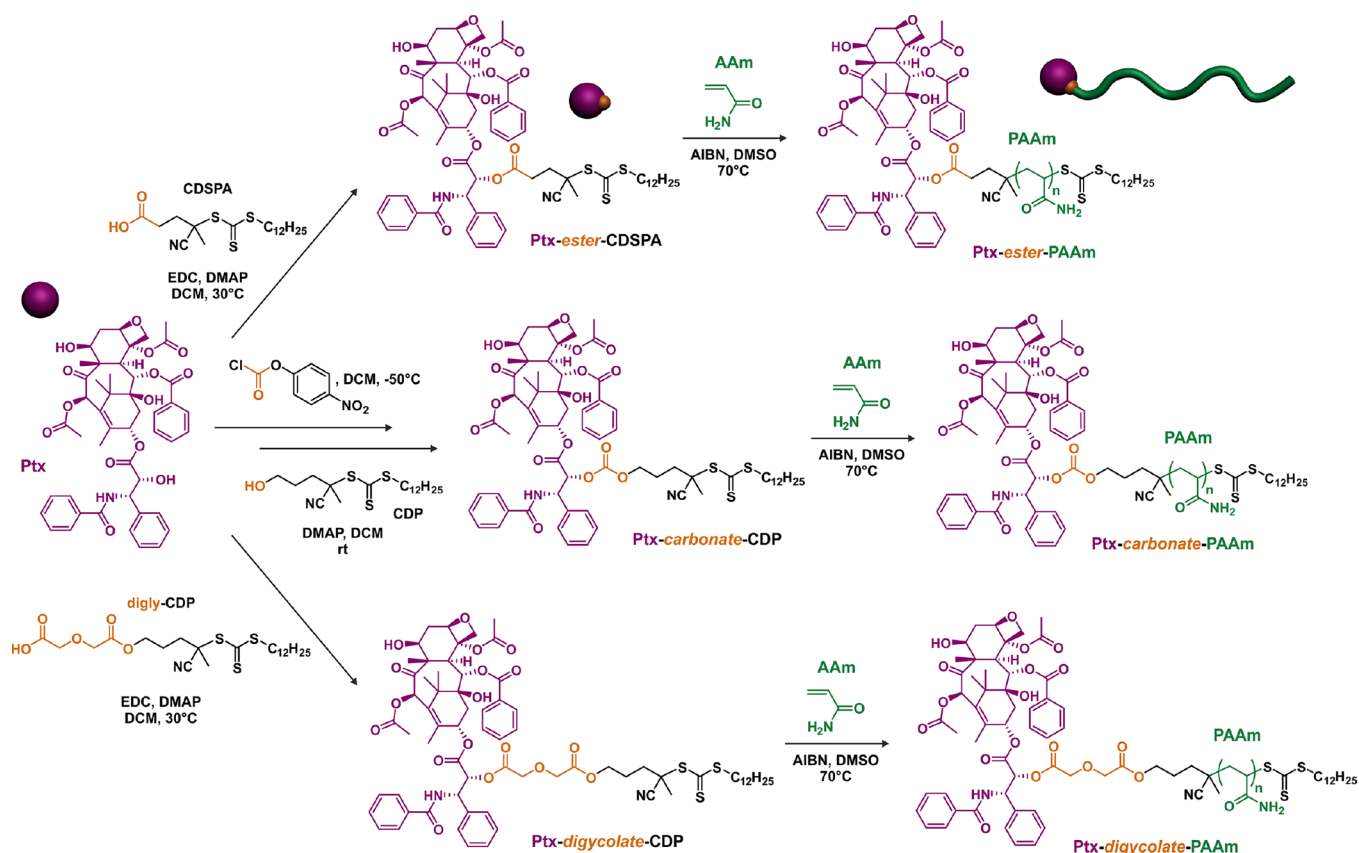
Figure 3. Synthesis of water-soluble, paclitaxel-polyacrylamide (Ptx-PAAm) prodrugs with ester, carbonate, or diglycolate linkers by RAFT polymerization of acrylamide (AAm) from the Ptx-*ester*-CDSPA, Ptx-*carbonate*-CDP, or Ptx-*diglycolate*-CDP RAFT agent, respectively.

USA), and samples were put in an oven at 60 °C overnight. They were then whitewashed by adding twice 100 μL of H_2O_2 30% (w/v) and warmed for 30 min at 60 °C in an oven. Finally, plasma and treated organ samples were mixed with Ultimagold (PerkinElmer, USA) and radioactivity was measured with a LS 6500 multipurpose scintillation counter (Beckman Coulter). Radioactive counting allowed access to total Ptx concentration and metabolites: [total Ptx] = [free Ptx] + [Ptx-*ester*-PAAm] + [Ptx metabolites]. Pharmacokinetic parameters were determined using PKSolver.[32]

Anticancer Efficacy. 52 healthy female BALB/c nude mice, 6−8 weeks old, were obtained from Charles River. After 2 weeks of acclimation, MCF-7 breast tumors were induced by subcutaneous injection of 10 × 10^6 MCF-7 cells in 200 μL of RPMI 1640 medium into the right flank of mice. At day 17, when tumors reach a mean volume of 100−150 mm^3, 40 animals out of 52 were randomized into 4 groups of 9 animals each. Homogeneity of the mean tumor volume between groups was tested by an analysis of variance (ANOVA). The treatments started the day of randomization. Treatment was administered either by SC injection in the interscapular region or by IV injection into the caudal vein. A Q7Dx3 treatment schedule was applied as follows: (i) PAAm SC at 1520 mg kg^{-1}, once a week 3 consecutive times (negative control); (ii) Ptx-*ester*-PAAm SC at 15 mg kg^{-1} (Taxol equivalent dose); (iii) Ptx-*ester*-PAAm SC at 60 mg kg^{-1} (Taxol equivalent dose), which corresponds to Ptx-PAAm maximal tolerated dose; and (iv) Taxol IV at 15 mg kg^{-1} (Taxol maximal tolerated dose). Animal viability and behavior were observed daily, and body weights were measured twice a week. Tumor volume was measured twice a week with a caliper and estimated with the following formula: volume = (length × width^2)/2. Mice were euthanized by overdosage on gas anesthesia (isoflurane) followed by cervical dislocation when Humane endpoints were reached.[33,34]

Statistics. Statistics were performed using GraphPad Prism (version 8.0.2). Comparison of tumor growth results between groups was analyzed for statistical significance, using two-way ANOVA, with Tukey's multiple post-hoc comparisons.

■ RESULTS AND DISCUSSION

Preliminary Screening of Different Water-Soluble Polymers. Knowing that the nature of the polymer would play a key role in the physicochemical properties and in vivo fate of the polymer prodrugs, we sought to perform a preliminary screening in terms of pharmacokinetics and biodistribution of a small library of water-soluble polymers frequently used in nanomedicine,[35−37] in order to select the polymer with the best performances once in blood circulation. As potential candidates (Figure 2a), we selected the following: (i) linear PEG, which is the most used polymer in bioconjugation and nanomedicine;[38] (ii) POEGMA, as a well-known alternative to linear PEG;[39] (iii) PHPMA, which has been extensively investigated to prepare polymer prodrugs;[40] (iv) PMPC, a stealth, zwitterionic polymer with even better performances than PEG;[41,42] and (v) PAAm, which is highly water-soluble, biocompatible and also exhibits stealth properties.[24,25,35]

All polymers were fluorescently labeled by functionalizing them with Cy5.5 (Figure 2b), a near-infrared-emitting dye suitable for in vivo imaging. While **Cy5.5-PEG** was obtained by coupling Cy5.5 to a α-NHS-PEG (M_n = 23 kg mol^{-1}) by amidification reaction, **Cy5.5-POEGMA**, **Cy5.5-PHPMA**, **Cy5.5-PMPC**, and **Cy5.5-PAAm$^{20 k}$** (M_n = 15−19 kg mol^{-1}) were obtained by reversible addition-fragmentation chain transfer (RAFT) polymerization from NHS-CEP as a RAFT agent followed by coupling to Cy5.5 (see the experimental

section). After normalization of the fluorescence, the Cy5.5-polymers were injected intravenously to breast tumor-bearing mice, and fluorescence imaging was performed at different time points. From the results, **Cy5.5-PAAm$^{20 \text{ k}}$** exhibited both the longest circulation time and the greatest tumor accumulation (Figure 2c). The latter point was also confirmed by ex vivo biodistribution performed after 48 h and 14 days (Figure 2d and Figure S1), showing higher fluorescence intensity in tumors for **Cy5.5-PAAm$^{20 \text{ k}}$** compared to other polymers. Moreover, ex vivo imaging of tumor sections passing through their centers revealed greatest tumor penetration of **Cy5.5-PAAm$^{20 \text{ k}}$** compared to other polymers (Figure 2e,f). In fact, a PAAm of $M_n \sim 20$ kg mol^{-1} appeared to be a good compromise in terms of drug loading vs circulation time/tumor accumulation since reduction of its M_n to 7.0 and 4.2 kg mol^{-1} led to rapid clearance as early as 24 h (Figure S2) and very little tumor accumulation (Figures S3 and S4).

In conclusion of this screening study, we considered that PAAm had the most advantageous properties for the intended application that requires high water solubility, stealth properties, and ideally high tumor accumulation/penetration and that the previously developed Ptx-POEGMA polymer prodrugs[30] would have very likely shown inferior performances.

Synthesis and Characterization of Water-Soluble Ptx-PAAm Polymer Prodrugs. After having selected PAAm as the best water-soluble polymer, the polymer prodrugs were synthesized by the "drug-initiated" method,[43] which relies on the controlled growth of a polymer chain from a drug derivatized by a polymerization initiator/controlling agent to perform controlled polymerization. This strategy was chosen to facilitate clinical translation because it of its simplicity and scalability as well as simplified workup since only the unreacted monomer (which is often volatile) needs to be removed. Conversely, the opposite strategy, which consists of coupling drugs to preformed polymers (termed "grafting to"), often exhibits incomplete coupling efficiencies and requires tedious purification due to the difficulty in separating two types of macromolecules (i.e., unreacted polymer and the polymer prodrugs), and/or removing unreacted drug and coupling agent. The "drug-initiated" method is also very robust and flexible since it is easily applicable to different drugs/linkers/polymers,[30,44−47] leading to a broad range of different polymer prodrugs with tunable drug delivery properties.

A small library of well-defined Ptx-PAAm prodrugs was synthesized by RAFT polymerization of AAm using Ptx-based, trithiocarbonate chain transfer agents (Figure 3 and Figure S5). Three different linkers were investigated (ester, carbonate, and diglycolate) to find the optimal balance in terms of linker stability vs lability to prevent early drug release into the SC tissue while ensuring its release into the blood before prodrug excretion (Figures 2b and 3). These linkers were chosen for their sensitivity to circulating enzymes with esterase activity and with moderate expression variability in humans, thus ensuring comparable interpatient drug release patterns.[48,49]

Ptx-*ester*-PAAm was obtained by coupling Ptx to CDSPA as a chain transfer agent (Figure 3 and Figure S5a) followed by RAFT polymerization at 70 °C in DMSO using AIBN as the initiator (Figure 3 and Figure S6). By adjusting the $[\text{AAm}]_0/[\text{Ptx-}ester\text{-CDSPA}]_0$ ratio from 53 to 266, the PAAm chain length was varied to determine the minimal M_n that allows for complete solubilization of the prodrug in water, which is a prerequisite to preventing SC toxicity and warranting high SC bioavailability. ^{1}H NMR spectroscopy of the purified prodrugs

showed all expected signals, especially amide, methylene, and methine protons from the PAAm backbone together with aromatic and characteristic protons from Ptx (Figure S6).

The prodrugs exhibited $M_{n,\text{NMR}}$ ranging from 6200 to 21,600 g mol^{-1} in rather good agreement with $M_{n,\text{SEC}}$ values (**P1e−P3e**, Table 1 and Figure S7) and low dispersities ($Đ = 1.07-1.28$), thus accounting for a controlled polymerization process. By tuning the PAAm chain length, the drug loading varied from ~14 to ~4 wt %. Whereas **P1e** and **P2e** were only partially soluble in water at 3 mg mL^{-1} equiv Ptx because of the too short PAAm chains, **P3e** ($M_{n,\text{NMR}} = 21,600$ g mol^{-1}) was fully water-soluble at this equiv. Ptx concentration, which represents a 104-fold increase in solubility compared with free Ptx. Interestingly, since water solubility is a key parameter for SC administration and since PEG is still considered the gold standard for water-soluble, biocompatible polymers, we synthesized a Ptx-PEG of 23 kg mol^{-1} (Figure S8a) and compared its solubility to that of Ptx-PAAm **P3e** in water at 100 mg mL^{-1}. After solubilization of the prodrugs and centrifugation at 14,000 rpm, the Ptx-PEG solution led to important sedimentation, conversely to Ptx-PAAm whose solution stayed clear and homogeneous (Figure S8b). Since sedimentation/aggregation must be avoided in the SC tissue, this experiment further confirmed that PEG, despite its widespread use in nanomedicine, may not be the best polymer, as opposed to PAAm, for this type of application/prodrug system.

The structure of the RAFT agent was then modified to change the nature of the Ptx-PAAm linker. Previous reports have shown that diglycolate-based linkers are highly labile in plasma with faster release kinetics than the ester counterparts,[30,46,50] whereas carbonate linkers have shown slower release kinetics.[51] Therefore, well-defined Ptx-*carbonate*-PAAm (**P3c**) and Ptx-*diglycolate*-PAAm (**P3d**) of similar M_n to that of **P3e** were synthesized (Figures S5−S7, Table 1). They were obtained by following an identical polymerization procedure to that of the Ptx-*carbonate*-CDP and Ptx-*diglycolate*-CDP functional RAFT agents, respectively (Figure 3). Those were synthesized by activation of Ptx by 4-nitrophenyl chloroformate followed by reaction with CDP or by coupling Ptx to *diglycolate*-CDP.

Successful clinical translation requires simple and robust manufacturing methods that ensure the preparation of newly developed materials in large scales and with a high level of purity.[52] In this context, we also performed a multigram-scale synthesis of **P3e** where 4.8 g of Ptx-*ester*-CDSPA and 17.6 g of the corresponding polymer prodrug ($M_{n,\text{NMR}} = 24,000$ g mol^{-1}, $M_{n,\text{SEC}} = 24,780$ g mol^{-1}, $Đ = 1.17$) were obtained, with an overall yield of 60%. The high purity of **P3e** was assessed by HPLC, leading to residual amounts of free AAm and Ptx both below 1 ppm, much lower than the average dietary intake of AAm (1 μg kg^{-1} body weight day^{-1})[53] and below the threshold established by the European Medicines Agency for AAm in cosmetics.[54]

Physicochemical Characteristics and In Vitro Evaluation. Prior to performing biological evaluations, key physicochemical characteristics were investigated: (i) the viscosity and injectability of the prodrugs in aqueous solution, to ensure they can be injected under standard conditions used for SC administration, and (ii) the release kinetics of Ptx from the prodrugs in different media, to assess its fine tuning depending on the prodrug's structure.
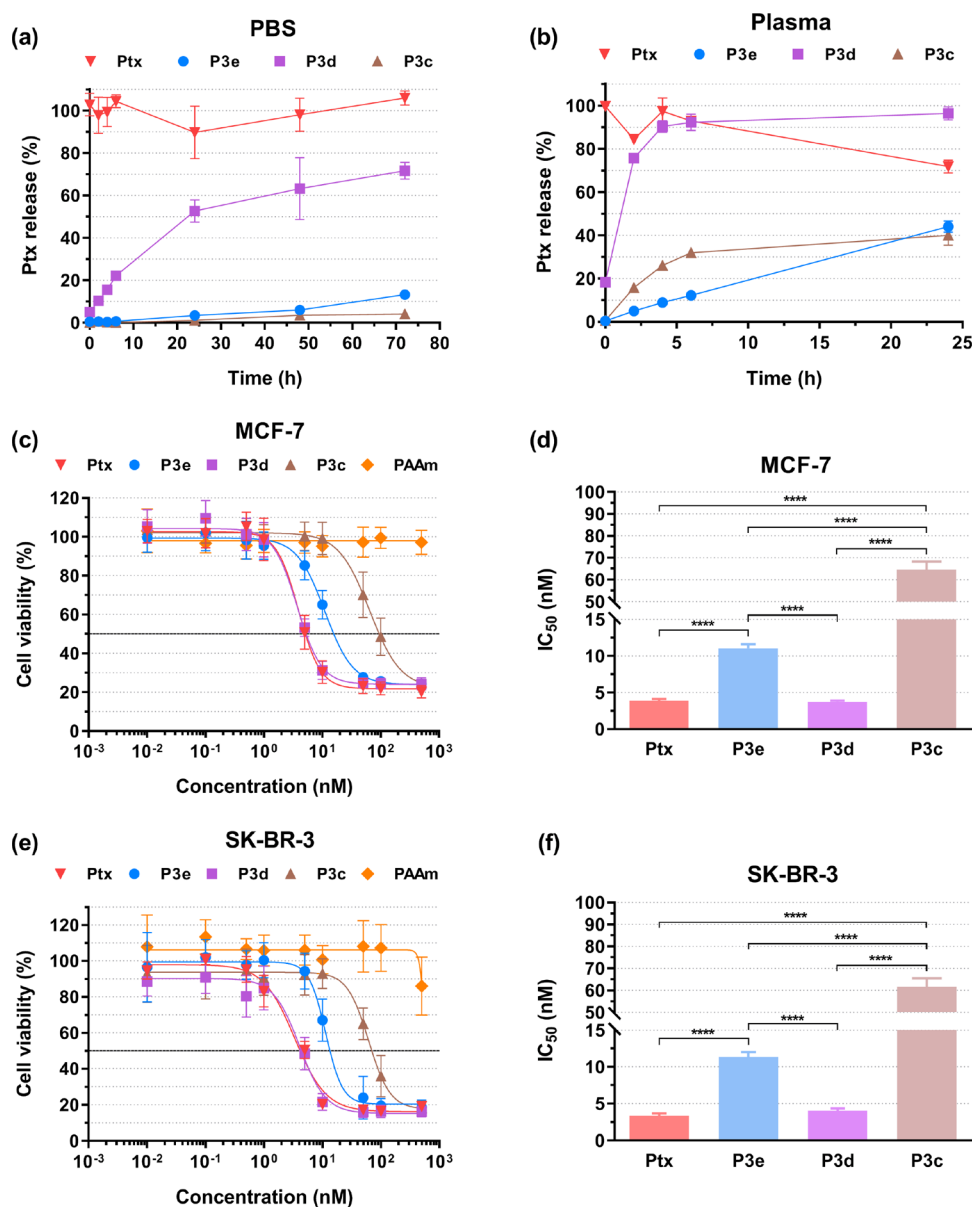
Figure 4. Ptx release profiles from **P3e**, **P3d**, and **P3d** (Ptx is plotted as the reference) in (a) PBS at 37 °C and (b) murine plasma at 37 °C. Cell viability (MTT test) with increasing concentrations of Ptx, **P3e**, **P3d**, **P3d**, and PAAm on (c) MCF-7 cells with (d) the corresponding IC_{50} and (e) SK-BR-3 cells with (f) the corresponding IC_{50} values. The values are expressed as the means ± SD. Unpaired two-tailed t test; ****$p < 0.0001$.

Measuring the viscosity and injectability (i.e., force required for injection) of the prodrugs in aqueous solution is of crucial importance as the maximum volume generally accepted for an SC injection is ~2 mL, thus requiring administration of the relatively concentrated solutions to reach the same dose regimens as the IV-administered counterparts. Whereas the viscosity of PAAm ($M_{n,SEC}$ = 37,000 g mol^{-1}, Đ = 1.10) synthesized by the same procedure was close to that of water (<10 cP) at 50 mg mL^{-1}, viscosity of **P3e** was ~200 cP at 50 mg mL^{-1} and increased to ~1 × 10^4 cP at 200 mg mL^{-1} (Figure S9). This is due to the presence of strongly hydrophobic Ptx moieties that induce the formation of hydrophobic domains, via Ptx−Ptx and likely Ptx−C$_{12}$ alkyl interactions, decreasing the mobility of the polymer chains.

The injectability of aqueous solutions of **P3e**, **P3d**, and **P3c** was measured as the function of the concentration with a 26 G × $^1/_2$″ needle as the preferred needle size for humans is ~25−

27 G. Up to 50 mg mL^{-1}, injection of the polymer prodrugs required a very low force of ~1 N, which was comparable to that of PAAm (Figure S10). Despite an increase in viscosity with the polymer prodrug concentrations, a concentration as high as ~130 mg mL^{-1} was achieved (corresponding to ~6 mg mL^{-1} in Ptx) at 30 N, which is the maximum acceptable injection force for SC administration.[55]

The release of Ptx from the prodrugs **P3c**, **P3d**, and **P3e** was then monitored in PBS and in murine plasma at 37 °C to investigate the influence of both the nature of the linker and of the medium (i.e., hydrolytic vs hydrolytic + enzymatic cleavage) on the release kinetics. The diglycolate moiety of **P3d** showed a dual hydrolytic/enzymatic susceptibility, resulting in the fastest release of Ptx in both media (~50% in PBS after 20 h and ~90% in plasma after 5 h) (Figure 4a,b). By comparison, **P3e** and **P3c** were both stable in PBS up to at least 70 h and gave comparable Ptx release kinetics in plasma
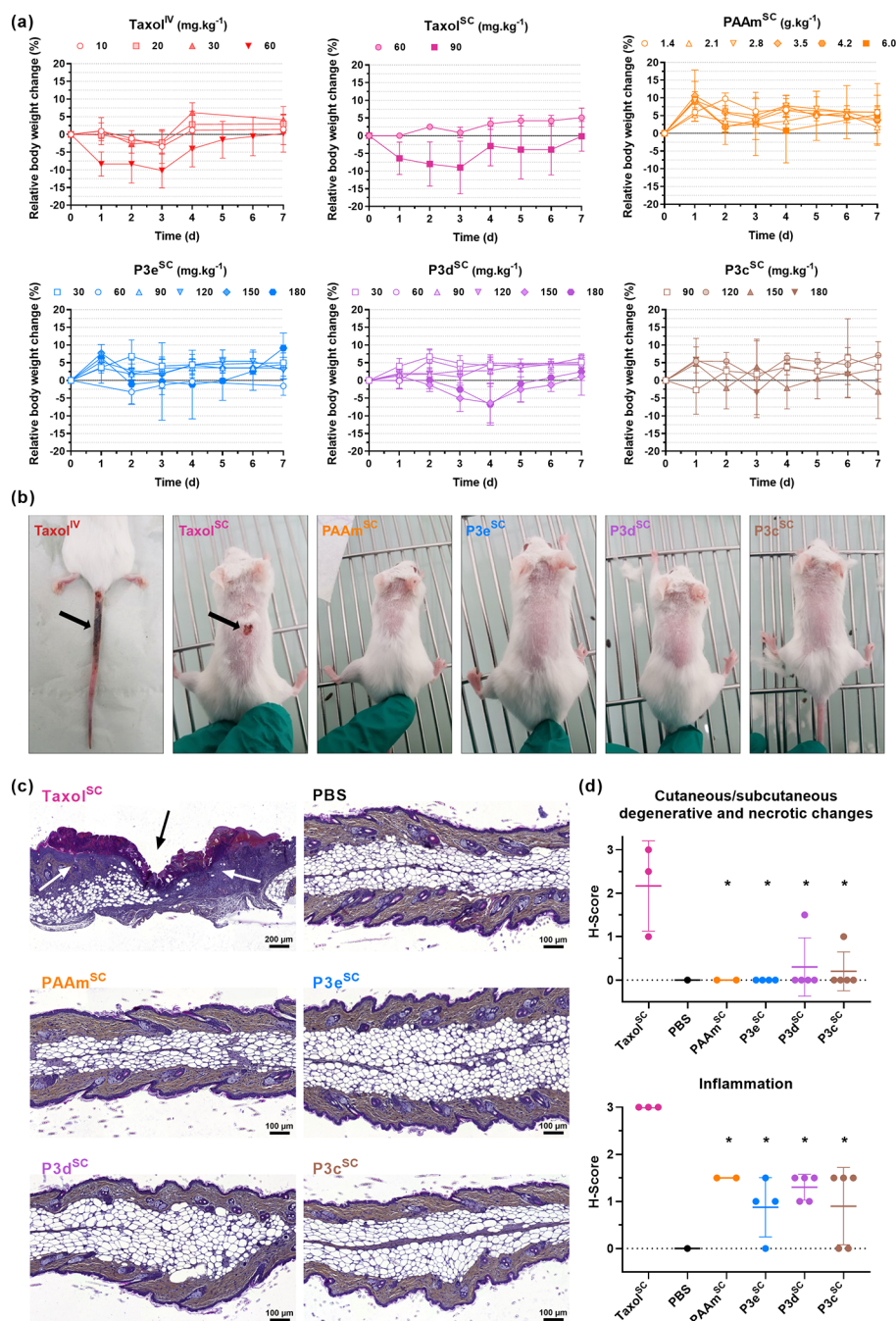
Figure 5. (a) Relative body weight change of mice as a function of time after IV injection of Taxol (Taxol^{IV}) and SC injection of Taxol (Taxol^{SC}), PAAm (PAAm^{SC}), **P3e** (**P3e**^{SC}), **P3d** (**P3d**^{SC}), and **P3c** (**P3c**^{SC}). The values are expressed as the means ± SD ($n = 3$). (b) Representative pictures of mice ($n = 3$) 7 days after injection of Taxol^{IV} at 60 mg kg^{-1}, Taxol^{SC} at 60 mg kg^{-1}, PAAm^{SC} at 4.2 g kg^{-1}, and **P3e**^{SC}, **P3d**^{SC}, and **P3c**^{SC} at 180 mg kg^{-1} (equiv Ptx). The black arrows indicate necrotic areas. (c) Representative HES-stained sections of skin samples from mice removed at the injection site after injection of Taxol^{SC} at 90 mg kg^{-1}, PBS, PAAm^{SC} at 4.2 g kg^{-1}, and **P3e**^{SC}, **P3d**^{SC}, and **P3c**^{SC} at 180 mg kg^{-1} (equiv Ptx). The black/white arrows indicate the severe cutaneous necrosis, only observed after SC injection of Taxol at 90 mg kg^{-1}. (d) Histopathological scoring (H-Score) of degenerative/necrotic changes and tissular inflammation in mice after injection of Taxol^{SC} at 90 mg kg^{-1}, PAAm^{SC} up to 4.2 g kg^{-1}, and **P3e**^{SC}, **P3d**^{SC}, and **P3c**^{SC} up to 180 mg kg^{-1} (equiv Ptx). The values are expressed as the means ± SD. Unpaired two-tailed t test between the Taxol^{SC} group and the PAAm^{SC}, **P3e**^{SC}, **P3d**^{SC}, or **P3c**^{SC} group; *$p < 0.05$. See all pictures and individual scores in Figure S11 and Table S1.

(~40% after 24 h). Release kinetics were not monitored beyond 24 h in plasma due to the documented degradation of Ptx under these conditions.[56,57]

To assess whether the drug release profiles observed in plasma correlate with the cytotoxicity of the prodrugs, cell viability experiments were performed by measuring the mitochondrial activity via MTT assay on two breast cancer

cell lines (MCF-7 and SK-BR-3), corresponding to clinically relevant cancer models for Ptx. Importantly, all prodrugs led to significant cytotoxicity on both cell lines and their IC$_{50}$ values were in the following order: **P3d** < **P3e** < **P3c**. While PAAm was not cytotoxic (> 75% cell viability) up to 500 nM on both cell lines, free Ptx gave an IC$_{50}$ as low as 5 nM (Figure 4c−f). Since Ptx must be released from the prodrug before passively
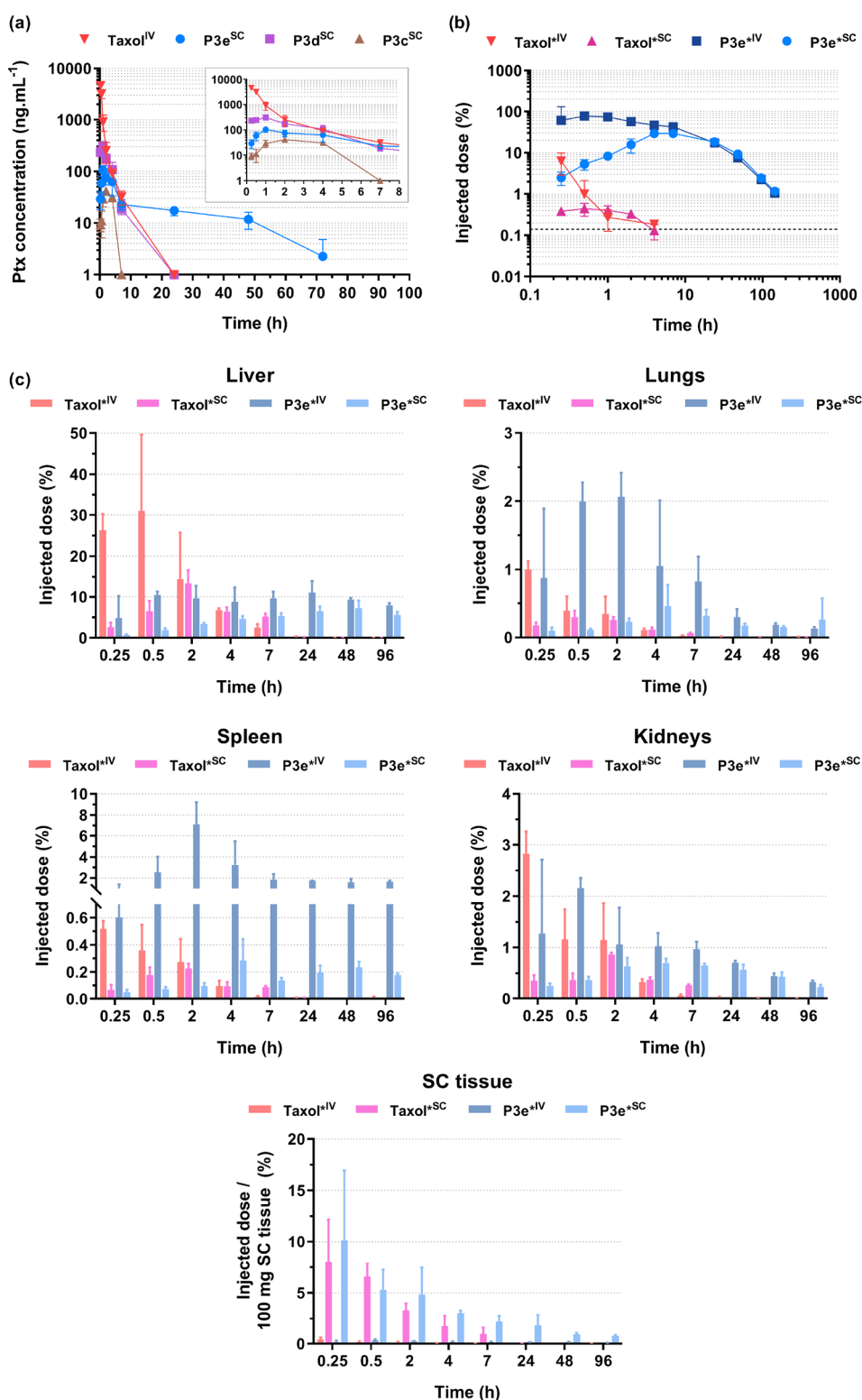
Figure 6. (a) Plasma concentration of free Ptx with time after injection of Taxol[IV], Taxol[SC], **P3e**[SC], **P3d**[SC], and **P3c**[SC] at 7 mg kg^{-1} equiv Ptx determined by LC−MS/MS (insert: zoomed-in region in the 0−10 h range). The values are expressed as the means ± SD (n = 4). (b) Plasma concentration and (c) biodistribution (in the liver, lungs, spleen, kidneys, and SC tissue) with time of total Ptx after injection of Taxol*[IV], Taxol*[SC], **P3e***[IV], and **P3e***[SC] at 7 mg kg^{-1} equiv Ptx determined by radioactive counting. The values are expressed as the means ± SD (n = 4). The horizontal dashed line represents the limit of quantification (0.14%).

diffusing through the cell membranes to reach the microtubules, slow release in plasma might be correlated with a high IC$_{50}$. It is also interesting to note that (i) due to the high lability of the diglycolate linker, **P3d** has the same IC$_{50}$ as that

of free Ptx and (ii) despite similar drug release profiles for **P3c** and **P3e** in PBS and plasma, **P3e** led to a much lower IC$_{50}$ than **P3c**, possibly due to differences in the enzymatic composition of murine plasma and cell culture medium.

Systemic and Acute Local Toxicity. The systemic toxicity of the prodrugs was then examined in mice to evaluate the MTD (i.e., the threshold at which all animals survived with a body weight loss lower than 10%) to find optimized treatments followed by evaluation of the acute local toxicity at the injection site (Figure 5).

Increasing concentrations of free PAAm and prodrugs **P3e**, **P3d**, and **P3c** were SC-injected (PAAm^{SC}, **P3e**^{SC}, **P3d**^{SC}, and **P3c**^{SC}, respectively) to healthy mice (single injection) followed by monitoring of their body weight and their behavior for 7 days (Figure 5a). The same protocol was applied to SC and IV injections of Taxol (Taxol^{SC} and Taxol^{IV}, respectively). Whereas Taxol^{IV} led to an MTD of 60 mg kg^{-1}, Taxol^{SC} reached 90 mg kg^{-1}, probably due to a decrease in C_{max} compared with IV administration and thus a dose-limiting reduction in C_{max}-related.[58] Mice treated with free PAAm^{SC} showed no sign of systemic toxicity up to a concentration as high as 6000 mg kg^{-1}, in good agreement with its well-documented biocompatibility/safety. Importantly, all prodrugs were successfully SC-injected up to at least 180 mg kg^{-1} equiv Ptx without exceeding a body weight loss of 10%. Neither mortality nor noticeable modification in terms of feeding and behavior was observed, thus suggesting the absence of systemic toxicity. Notably, the MTD was increased by at least a factor of 3 and 2 compared to Taxol^{IV} and Taxol^{SC}, respectively.

Similar to free PAAm^{SC}, none of the prodrugs showed local toxicity at and near the injection site up to 180 mg kg^{-1} equiv Ptx (Figure 5b). This observation likely ruled out early Ptx release in the SC tissue from the prodrugs even from **P3d**^{SC} that contains the most labile linker. Conversely, Taxol^{IV} and Taxol^{SC} led to significant ulceration and necrosis of the mice skin tissue at 60 mg kg^{-1} (see black arrows in Figure 5b), in agreement with the literature.[59] Histopathological examination of HES-stained sections of skin samples removed at the injection site confirmed the abovementioned macroscopic observations (Figure 5b). SC administration of the different polymer prodrugs evidenced a preserved architectural structure of the skin/SC tissue, with only focal small granulomatous lesion along the needle tract. Neither significant degenerative or necrotic tegumentary changes, nor inflammatory reaction, associated with the polymer prodrugs injection, was observed. On the contrary, Taxol^{IV} and especially Taxol^{SC} induced marked to severe ulcerative dermatitis with epidermal changes including hyperplasia and hyperkeratosis or severe epidermal–dermal necrosis replaced by a sero-cellular crust. Deep dermal and hypodermal inflammation was observed, granulomatous and/or granulocytic, associated with pannicular cytosteatonecrosis. Altogether, these results establish for the first time the possibility to safely administer a vesicant/irritant anticancer drug by SC injection.

Pharmacokinetics and Biodistribution. The biological fate of the prodrugs was then evaluated in terms of pharmacokinetics and biodistribution in mice. A first pharmacokinetic study based on LC–MS/MS allowed monitoring the evolution with time of the Ptx concentration coming from Taxol^{IV} or released from the prodrugs at 7 mg kg^{-1} equiv Ptx after SC administration. Taxol^{IV} exhibited a high C_{max} of 4660 ng mL^{-1} 15 min post-administration (t_{max}) followed by rapid clearance with undetectable amounts in plasma after 24 h (Figure 6a), in good agreement with previous pharmacokinetic studies of Taxol.[60] Conversely, the C_{max} values of **P3d**^{SC}, **P3e**^{SC}, and **P3c**^{SC} were lowered by at least an order of magnitude, to reach 310, 105, and 41 ng mL^{-1},

respectively (Table 2). These results are in agreement with the MTD of the prodrugs from the toxicity study (Figure 5) as

Table 2. Main Pharmacokinetic Parameters of Free Ptx Determined by LC–MS/MS after IV Injection of Taxol (Taxol^{IV}) at 7 mg kg^{-1} and after SC Injection of P3d^{SC}, P3e^{SC}, and P3c^{SC} at 7 mg kg^{-1} (Ptx equiv)

parameter	Taxol^{IV}	P3d^{SC}	P3e^{SC}	P3c^{SC}
$t_{1/2}$ (h)	1.7	1.5	13.9	1.6
t_{max} (h)	0.25	1	1	2
C_{max} (ng mL^{-1})	4657	310	105	41
AUC$_{0\rightarrow\infty}$ (ng mL^{-1} h)	4631	986	1299	186
MRT (h)	0.9	2.5	22.2	3.3
apparent bioavailability^a (%)	100	21	28	4

^{a}Determined according to AUC$_{0\rightarrow\infty}$/AUC$_{0\rightarrow\infty}$ IV.

lower C_{max} values led to decreased toxicity and thus enabled a higher MTD than Taxol.[58,61,62] Interestingly, the C_{max} values were observed at ~1–2 h (t_{max}) for all prodrugs. This delayed t_{max} compared to that of Taxol^{IV} is attributed to the time required for the prodrugs to be absorbed into the blood or lymphatic capillaries, combined with the prolonged release of Ptx from the prodrugs once they reach the bloodstream. Notably, **P3e**^{SC} showed a very different PK profile to the other prodrugs and Taxol^{IV}. Whereas the elimination half-lives ($t_{1/2}$) of **P3d**^{SC}, **P3c**^{SC}, and Taxol^{IV} were in the range of 1.5–1.7 h, the $t_{1/2}$ of **P3e**^{SC} approached 14 h and it was detectable for more than 3 days. The mean residence time (MRT) was also much higher for **P3e**^{SC} (22.2 h vs 0.9–3.3 h).

The apparent bioavailability of Ptx for **P3d**^{SC}, **P3e**^{SC}, and **P3c**^{SC} amounted to 21%, 28%, and 4% relative to Taxol IV, respectively (Table 2). This makes **P3e**^{SC} the best candidate as it possessed both the most suitable PK profile and the highest apparent bioavailability. Despite similar apparent bioavailability to **P3e**^{SC} and **P3d**^{SC}, **P3d**^{SC} exhibited a lower MRT and rapid release of Ptx once in the blood, leading to a too rapid clearance of the drug. For **P3c**^{SC}, Ptx was released too slowly and the prodrug was therefore excreted before it could effectively release its payload. The optimal performance of **P3e**^{SC} could be explained by its intermediate Ptx release profile in vivo (probably due to the presence of specific enzymes such as esterases), combined with the stealth properties provided by PAAm.[24,25,35] This resulted in a long circulating prodrug acting as a slow-release reservoir of Ptx. These results are important not only because they confirm that the nature of the linker plays a key role in the pharmacokinetics of Ptx but also because they show that bioavailability does not correlate linearly with the drug release pattern; thus, screening each prodrug in vivo was necessary.

P3e was then selected for further study. A radiolabeled counterpart (**P3e***) was synthesized from [H^3]-Ptx and used in a second pharmacokinetic study at the same dose to monitor the whole amount of Ptx in comparison to that of radiolabeled Taxol* (Figure 6b). Since quantification is performed by radioactivity counting, free [H^3]-Ptx, **P3e***, and their metabolites were dosed all together, which allows the fate of the prodrug to be followed. Free [H^3]-Ptx administered intravenously (Taxol*^{IV}) was rapidly cleared from the blood compartment (<1% of the injected dose still circulating at 30 min post-injection, Figure 6b) and exhibited most of the pharmacokinetic parameters similar to those previously observed by LC–MS/MS (Table 2). In comparison, Taxol*^{SC}
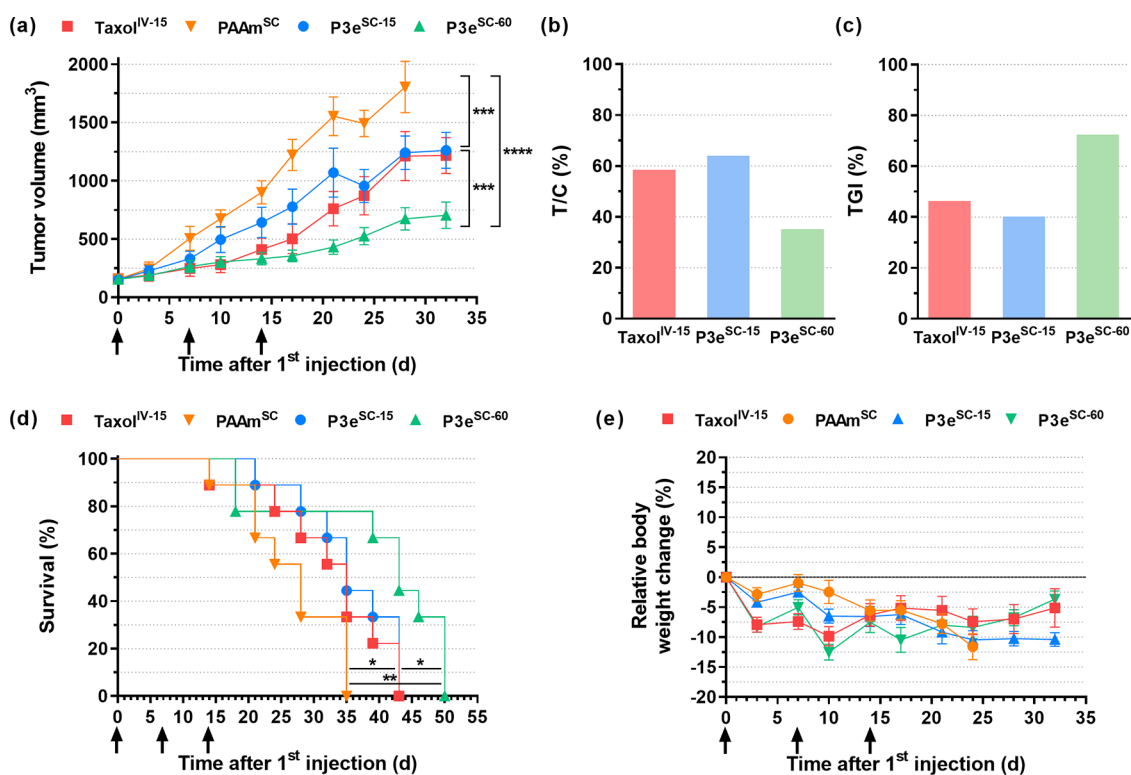
Figure 7. (a) Tumor growth evolution with time [the values are expressed as the means ± SEM (n = 9 per group). Two-way ANOVA, with Tukey's correction for multiple comparisons between groups at days 28 and 32; ***$p \leq 0.002$, ****$p < 0.0001$; (b) mean tumor volume over control volume (T/C) and (c) mean tumor growth inhibition (TGI) 10 days after treatment termination (d = 24 after 1st injection); (d) survival percentage evolution with time [Mantel−Cox test; *$p < 0.05$, **$p < 0.01$] and (e) weight evolution with time [the values are expressed as the means ± SEM (n = 9 per group)] of mice bearing MCF-7 xenografts after injection of Taxol^{IV}, PAAm^{SC} at 1520 mg kg^{-1}, **P3e^{SC}** at 15 mg kg^{-1} (**P3e^{SC-15}**), and **P3e^{SC}** at 60 mg kg^{-1} (**P3e^{SC-60}**) equiv Ptx, on days 0, 7, and 14 (black arrows).

showed a delayed entrance into the blood circulation, as shown by its very low C_{max} (<1% of the injected dose) and bioavailability of 25%. Ptx from IV-injected **P3e*** (**P3e*^{IV}**) has a prolonged circulation time with $t_{1/2}$ 10 times and AUC 100 times greater than Taxol*^{IV} (Table S2). Remarkably, Ptx from SC-injected **P3e*** (**P3e*^{SC}**) exhibited a high bioavailability (84% relative to **P3e*^{IV}**) and a total dose slowly increasing over time, from 3% of the injected dose 15 min post-injection up to 46% after 4 h. Once in the blood compartment, the prodrug remained in circulation for a prolonged period of time (MRT ~36 h), with a final Ptx blood concentration of still ~1% of the injected dose 6 days after injection, similar to that of **P3e*^{IV}**. It is worth noting that **P3e*^{SC}** and **P3e*^{IV}** exhibited the same $t_{1/2}$ value of ~25 h, revealing that the absorption rate is not significant after 24 h, suggesting quantitative absorption of **P3e*^{SC}** into the blood within this period of time.

From the biodistribution study into key organs, both **P3e*^{SC}** and **P3e*^{IV}** showed very limited accumulation in the liver (<10% of the injected dose) 48 h post-injection, compared to 30% of the injected dose for Taxol*^{IV} after 30 min, presumably as a result of the stealth properties of the prodrugs (Figure 6c). For other organs (lungs, spleen, kidneys), the total concentrations of Ptx from **P3e*^{SC}**, **P3e*^{IV}**, and Taxol*^{IV} were low and in the same range (except a modest accumulation of **P3e*^{IV}** in the spleen), revealing no noticeable acute toxicity. The total amount of Ptx from **P3e*^{SC}** was also monitored in the SC tissue. It decreased sharply over time, in parallel with an increase in the bloodstream, as shown from the pharmacokinetic profile (Figure 6c). The SC data further

prove the rapid blood passage of the hydrophilic prodrug from the SC tissue. Overall, taking into account the PK/BD data and the toxicity study, these results argue for efficacy studies of **P3e^{SC}** in mouse tumor models.

Anticancer Efficacy. An efficacy study was then designed to address two important points. Will **P3e^{SC}** be as efficient as Taxol^{IV} at the same dose? And if yes, can **P3e^{SC}** outperform Taxol^{IV} at a higher dose thanks to its higher MTD?

In this context, mice bearing MCF-7 xenografts were treated with (i) PAAm^{SC} at 1520 mg kg^{-1}, which would correspond to 60 mg kg^{-1} equiv Ptx for the prodrug counterpart; (ii) Taxol^{IV} at 15 mg kg^{-1}, determined to be the MTD for a weekly injection repeated over 3 weeks; and (iii) **P3e^{SC}** at two different doses, either 15 mg kg^{-1} equiv Ptx (to have the same dose as Taxol^{IV}) or at a 4 times higher dose of 60 mg kg^{-1} (determined to be the MTD in equivalent Ptx of **P3e^{SC}** for such a dose regimen). The antitumor efficacy of the different treatments was evaluated by following the tumor growth (Figure 7a), from which two key metrics used to characterize the antitumor activity were extracted:[63] the tumor volume over control volume (T/C) (Figure 7b) and the tumor growth inhibition (TGI) (Figure 7c). The overall survival of mice (Figure 7d) during the study and the mice body weight evolution (Figure 7e) were also monitored.

PAAm^{SC}-treated mice exhibited rapid tumor growth with an average tumor volume exceeding 1500 cm^3 ~40 days post-tumor induction (Figure 7a and Figure S12). Conversely, Taxol^{IV} and **P3e^{SC}** at 15 mg kg^{-1} both showed similar anticancer activity as attested by reduction on tumor growth compared to PAAm^{SC} (Figure 7a and Figure S12), together

with similar T/C (59−64%) and TGI (40−46%) values 10 days after treatment termination (Figure 7b,c and Tables S2 and S3). This first result is of crucial importance as, despite the lower apparent bioavailability of Ptx from **P3e^SC** (Table 2), the efficacy study revealed that it had a similar antitumoral activity to Taxol[IV] at the same dose. In combination with the toxicity data, this suggested a successful and safe transposition from IV-injected Taxol to SC-injected Ptx in the form of a water-soluble polymer prodrug.

Remarkably, when **P3e^SC** was administered at a higher dose of 60 mg kg^{-1} equiv Ptx, it displayed a dose-dependent anticancer activity and outperformed Taxol[IV] (Figure 7a and Figure S12) with a T/C as low as 35% and a much higher TGI value of 73% 10 days after treatment termination (Figure 7b,c and Tables S2 and S3). Consequently, not only was SC administration of **P3e** successful but it could also induce greater anticancer activity than Taxol[IV] thanks to its higher MTD.

In terms of overall survival of mice (Figure 7d), **P3e^SC** administered at 60 mg kg^{-1} equiv Ptx led to the highest survival rate of 78%, 25 days after treatment termination, whereas it was 44% for **P3e^SC** at 15 mg kg^{-1}, only 33% for Taxol[IV,] and 0% for the control group (PAAm^SC). As a result, **P3e^SC** more than doubled the survival rate compared to Taxol[IV]. The evolution of the relative body weight loss in **P3e^SC**-treated mice also revealed that the treatment was well tolerated as mice lost no more than 10% of their body weight throughout the efficacy study (Figure 7e).

CONCLUSIONS

In this work, we presented a novel and general approach for the SC administration of irritant/vesicant anticancer drugs via the design of well-defined hydrophilic polymer prodrugs constructed by the "drug-initiated" method. To validate our strategy, it was applied to the anticancer drug Ptx as a worst-case scenario due to its high hydrophobicity and vesicant/irritant properties. After a preliminary screening of well-established polymers used in nanomedicine, we selected PAAm as a water-soluble polymer owing to its greater water solubility, pharmacokinetic profile, and tumor accumulation/diffusion. A small library of Ptx-PAAm polymer prodrugs was then synthesized by varying the nature of the linker (ester, diglycolate, and carbonate) and choosing the appropriate chain length ($M_n \sim 20$ kg mol^{-1}) to obtain fully water-soluble polymer prodrugs. We then performed a comprehensive preclinical development of these polymer prodrugs by studying their physicochemical properties, drug release kinetics on two different cancer cell lines, and acute local and systemic toxicity as well as their pharmacokinetic and biodistribution profiles and anticancer efficacy in tumor-bearing mice of the most promising candidate (i.e., Ptx-*ester*-PAAm). We demonstrated that SC injection of hydrophilic polymer prodrugs based on Ptx as a representative vesicant/irritant anticancer drug allowed sustained release of Ptx in the bloodstream and outperformed the anticancer efficacy of Taxol, the commercial formulation of Ptx, without inducing local toxicity.

Given the flexibility of the synthetic approach, these achievements pave the way for SC administration of a wide range of anticancer drugs, including irritant and vesicant ones, and make it possible to safely consider the translation of many IV chemotherapies to SC chemotherapies. From a more general perspective, this new drug-delivery platform could also represent an important step toward self-administration and chemotherapy at home, which would greatly increase patient comfort and reduce the high cost of cancer treatment, the latter being crucial for low- and middle-income countries.

From a more general point of view, even if PAAm has already been investigated a little in nanomedicine as an alternative to PEG, we think that its use should be revisited because of its advantageous properties such as its high solubility in water, its stealth features, and its ease/flexibility of synthesis notably via reversible deactivation radical polymerization techniques that allow fine tuning of its macromolecular characteristics.

■ ASSOCIATED CONTENT

ⓢ Supporting Information

The Supporting Information is available free of charge at https://pubs.acs.org/doi/10.1021/jacs.2c04944.

<div style="margin-left:2em">

Ex vivo fluorescence imaging of organs, in vivo fluorescence imaging of mice, biodistribution from ex vivo fluorescence imaging, ^{1}H NMR of the Ptx-based RAFT agents, macromolecular characteristics (^{1}H NMR, SEC) and viscosity measurements of the polymer prodrugs, pictures of the mice used in the systemic toxicity study, individual scores of the local toxicity study, main PK parameters of radiolabeled Ptx, individual tumor growth evolution of mice during the efficacy study, evolution with time of tumor volume over control volume, and evolution with time of tumor growth inhibition (PDF)

</div>

■ AUTHOR INFORMATION

Corresponding Authors

Nicolas Tsapis − *Université Paris-Saclay, CNRS, Institut Galien Paris-Saclay, 91400 Orsay, France*; Email: nicolas.tsapis@universite-paris-saclay.fr

Julien Nicolas − *Université Paris-Saclay, CNRS, Institut Galien Paris-Saclay, 91400 Orsay, France*; ⓘ orcid.org/0000-0002-1597-0873; Email: julien.nicolas@universite-paris-saclay.fr

Authors

Alexandre Bordat − *Université Paris-Saclay, CNRS, Institut Galien Paris-Saclay, 91400 Orsay, France*; Present Address: Imescia, Université Paris-Saclay, 91400 Saclay, France

Tanguy Boissenot − *Université Paris-Saclay, CNRS, Institut Galien Paris-Saclay, 91400 Orsay, France*; Present Address: Imescia, Université Paris-Saclay, 91400 Saclay, France

Nada Ibrahim − *Université Paris-Saclay, CNRS, Institut Galien Paris-Saclay, 91400 Orsay, France*; Present Address: Imescia, Université Paris-Saclay, 91400 Saclay, France

Marianne Ferrere − *Université Paris-Saclay, CNRS, Institut Galien Paris-Saclay, 91400 Orsay, France*

Manon Levêque − *Université Paris-Saclay, CNRS, Institut Galien Paris-Saclay, 91400 Orsay, France*

Léa Potiron − *Imescia, Université Paris-Saclay, 91400 Saclay, France*

Stéphanie Denis − *Université Paris-Saclay, CNRS, Institut Galien Paris-Saclay, 91400 Orsay, France*

Sébastien Garcia-Argote − *Département Médicaments et Technologies pour la Santé (DMTS), SCBM, Université Paris-Saclay, CEA, INRAE, Gif-sur-Yvette F-91191, France*

Olivia Carvalho − *Département Médicaments et Technologies pour la Santé (DMTS), SCBM, Université Paris-Saclay, CEA, INRAE, Gif-sur-Yvette F-91191, France*

Jérôme Abadie − *Laboniris, Départment de Biology, Pathologie et Sciences de l'Aliment, Oniris, F-44307 Nantes, France*

Catherine Cailleau − *Université Paris-Saclay, CNRS, Institut Galien Paris-Saclay, 91400 Orsay, France*

Grégory Pieters − *Département Médicaments et Technologies pour la Santé (DMTS), SCBM, Université Paris-Saclay, CEA, INRAE, Gif-sur-Yvette F-91191, France;* ● orcid.org/0000-0002-3924-8287

Complete contact information is available at:
https://pubs.acs.org/10.1021/jacs.2c04944

Notes

■ ACKNOWLEDGMENTS

■ REFERENCES

(1) Stewart, B. W.; Wild, C. P. *World Cancer Report 2014*. International Agency for Research on Cancer: 2014.

(2) Weir, H. K.; Thompson, T. D.; Soman, A.; Møller, B.; Leadbetter, S.; White, M. C. Meeting the Healthy People 2020 Objectives to Reduce Cancer Mortality. *Prev. Chronic Dis.* **2015**, *12*, E104.

(3) Mariotto, A. B.; Robin Yabroff, K.; Shao, Y.; Feuer, E. J.; Brown, M. L. Projections of the Cost of Cancer Care in the United States: 2010−2020. *J. Natl. Cancer Inst.* **2011**, *103*, 117−128.

(4) *Drugwatch*. https://www.drugwatch.com/2015/10/07/cost-of-cancer (accessed 2022-10-04).

(5) Aitken, M., Kleinrock, M. *Global Oncology Trend Report*. IMS Institute for Healthcare Informatics: 2016.

(6) Koh, D. B. C.; Gowardman, J. R.; Rickard, C. M.; Robertson, I. K.; Brown, A. Prospective study of peripheral arterial catheter infection and comparison with concurrently sited central venous catheters. *Crit. Care Med.* **2008**, *36*, 397−402.

(7) Pujol, M.; Hornero, A.; Saballs, M.; Argerich, M. J.; Verdaguer, R.; Cisnal, M.; Peña, C.; Ariza, J.; Gudiol, F. Clinical epidemiology and outcomes of peripheral venous catheter-related bloodstream infections at a university-affiliated hospital. *J. Hosp. Infect.* **2007**, *67*, 22−29.

(8) Collins, D. S.; Sánchez-Félix, M.; Badkar, A. V.; Mrsny, R. Accelerating the development of novel technologies and tools for the subcutaneous delivery of biotherapeutics. *J. Controlled Release* **2020**, *321*, 475−482.

(9) Jin, J. F.; Zhu, L. L.; Chen, M.; Xu, H. M.; Wang, H. F.; Feng, X. Q.; Zhu, X. P.; Zhou, Q. The optimal choice of medication administration route regarding intravenous, intramuscular, and subcutaneous injection. *Patient Prefer. Adherence* **2015**, *9*, 923−942.

(10) Pivot, X.; Gligorov, J.; Müller, V.; Barrett-Lee, P.; Verma, S.; Knoop, A.; Curigliano, G.; Semiglazov, V.; López-Vivanco, G.; Jenkins, V.; Scotto, N.; Osborne, S.; Fallowfield, L. Preference for subcutaneous or intravenous administration of trastuzumab in patients with HER2-positive early breast cancer (PrefHer): an open-label randomised study. *Lancet Oncol.* **2013**, *14*, 962−970.

(11) Leveque, D. Subcutaneous Administration of Anticancer Agents. *Anticancer Res.* **2014**, *34*, 1579−1586.

(12) Sequeira, J. A. D.; Santos, A. C.; Serra, J.; Estevens, C.; Seiça, R.; Veiga, F.; Ribeiro, A. J. Subcutaneous delivery of biotherapeutics: challenges at the injection site. *Expert Opin. Drug Delivery* **2019**, *16*, 143−151.

(13) Laza-Knoerr, A. L.; Gref, R.; Couvreur, P. Cyclodextrins for drug delivery. *J. Drug Targeting* **2010**, *18*, 645−656.

(14) Heise, T.; Meiffren, G.; Alluis, B.; Seroussi, C.; Ranson, A.; Arrubla, J.; Correia, J.; Gaudier, M.; Soula, O.; Soula, R.; DeVries, J. H.; Klein, O.; Bode, B. BioChaperone Lispro versus faster aspart and insulin aspart in patients with type 1 diabetes using continuous subcutaneous insulin infusion: A randomized euglycemic clamp study. *Diabetes, Obes. Metab.* **2019**, *21*, 1066−1070.

(15) Frost, G. I. Recombinant human hyaluronidase (rHuPH20): an enabling platform for subcutaneous drug and fluid administration. *Expert Opin. Drug Delivery* **2007**, *4*, 427−440.

(16) Locke, K. W.; Maneval, D. C.; LaBarre, M. J. ENHANZE® drug delivery technology: a novel approach to subcutaneous administration using recombinant human hyaluronidase PH20. *Drug Delivery* **2019**, *26*, 98−106.

(17) McLennan, D. N.; Porter, C. J. H.; Charman, S. A. Subcutaneous drug delivery and the role of the lymphatics. *Drug Discovery Today Technol.* **2005**, *2*, 89−96.

(18) Chen, W.; Yung, B. C.; Qian, Z.; Chen, X. Improving long-term subcutaneous drug delivery by regulating material-bioenvironment interaction. *Adv. Drug Delivery Rev.* **2018**, *127*, 20−34.

(19) Oussoren, C.; Storm, G. Liposomes to target the lymphatics by subcutaneous administration. *Adv. Drug Delivery Rev.* **2001**, *50*, 143−156.

(20) Barbee, M. S.; Owonikoko, T. K.; Harvey, R. D. Taxanes: vesicants, irritants, or just irritating? *Ther. Adv. Med. Oncol.* **2013**, *6*, 16−20.

(21) Shenaq, S. M.; Abbase, E.-H. A.; Friedman, J. D. Soft-tissue Reconstruction Following Extravasation of Chemotherapeutic Agents. *Surg. Oncol. Clin. N. Am.* **1996**, *5*, 825−846.

(22) Alley, E.; Green, R.; Schuchter, L. Cutaneous toxicities of cancer therapy. *Curr. Opin. Oncol.* **2002**, *14*, 212.

(23) Boyle, D. M.; Engelking, C. Vesicant extravasation: myths and realities. *Oncol. Nurs. Forum* **1995**, *22*, 57−67.

(24) Kaneda, Y.; Tsutsumi, Y.; Yoshioka, Y.; Kamada, H.; Yamamoto, Y.; Kodaira, H.; Tsunoda, S.-i.; Okamoto, T.; Mukai, Y.; Shibata, H.; Nakagawa, S.; Mayumi, T. The use of PVP as a polymeric carrier to improve the plasma half-life of drugs. *Biomaterials* **2004**, *25*, 3259−3266.

(25) Torchilin, V. P.; Shtilman, M. I.; Trubetskoy, V. S.; Whiteman, K.; Milstein, A. M. Amphiphilic vinyl polymers effectively prolong liposome circulation time in vivo. *Biochim. Biophys. Acta, Biomembr.* **1994**, *1195*, 181−184.

(26) Yamauchi, P. S. Emerging permanent filler technologies: focus on Aquamid. *Clin. Cosmet. Investig. Dermatol.* **2014**, *7*, 261−266.

(27) Kinnunen, H. M.; Mrsny, R. J. Improving the outcomes of biopharmaceutical delivery via the subcutaneous route by understanding the chemical, physical and physiological properties of the subcutaneous injection site. *J. Controlled Release* **2014**, *182*, 22−32.

(28) Kingston, D. G. I. Taxol: The chemistry and structure-activity relationships of a novel anticancer agent. *Trends Biotechnol.* **1994**, *12*, 222−227.

(29) Hertz, D. L.; Kidwell, K. M.; Vangipuram, K.; Li, F.; Pai, M. P.; Burness, M.; Griggs, J. J.; Schott, A. F.; Van Poznak, C.; Hayes, D. F.; Lavoie Smith, E. M.; Henry, N. L. Paclitaxel Plasma Concentration after the First Infusion Predicts Treatment-Limiting Peripheral Neuropathy. *Clin. Cancer Res.* **2018**, *24*, 3602−3610.

(30) Bao, Y.; Guégain, E.; Mougin, J.; Nicolas, J. Self-stabilized, hydrophobic or PEGylated paclitaxel polymer prodrug nanoparticles for cancer therapy. *Polym. Chem.* **2018**, *9*, 687−698.

(31) Burckbuchler, V.; Mekhloufi, G.; Giteau, A. P.; Grossiord, J. L.; Huille, S.; Agnely, F. Rheological and syringeability properties of highly concentrated human polyclonal immunoglobulin solutions. *Eur. J. Pharm. Biopharm.* **2010**, *76*, 351−356.

(32) Zhang, Y.; Huo, M.; Zhou, J.; Xie, S. PKSolver: An add-in program for pharmacokinetic and pharmacodynamic data analysis in Microsoft Excel. *Comput. Methods Programs Biomed.* **2010**, *99*, 306−314.

(33) Sonnichsen, D. S.; Liu, Q.; Schuetz, E. G.; Schuetz, J. D.; Pappo, A.; Relling, M. V. Variability in human cytochrome P450 paclitaxel metabolism. *J. Pharmacol. Exp. Ther.* **1995**, *275*, 566−575.

(34) Gianni, L.; Kearns, C. M.; Giani, A.; Capri, G.; Viganò, L.; Lacatelli, A.; Bonadonna, G.; Egorin, M. J. Nonlinear pharmacokinetics and metabolism of paclitaxel and its pharmacokinetic/pharmacodynamic relationships in humans. *J. Clin. Oncol.* **1995**, *13*, 180−190.

(35) Knop, K.; Hoogenboom, R.; Fischer, D.; Schubert, U. S. Poly(ethylene glycol) in Drug Delivery: Pros and Cons as Well as Potential Alternatives. *Angew. Chem., Int. Ed.* **2010**, *49*, 6288−6308.

(36) Barz, M.; Luxenhofer, R.; Zentel, R.; Vicent, M. J. Overcoming the PEG-addiction: well-defined alternatives to PEG, from structure−property relationships to better defined therapeutics. *Polym. Chem.* **2011**, *2*, 1900−1918.

(37) Qi, Y.; Chilkoti, A. Protein−polymer conjugation−moving beyond PEGylation. *Curr. Opin. Chem. Biol.* **2015**, *28*, 181−193.

(38) Veronese, F. M.; Harris, J. M. Introduction and overview of peptide and protein pegylation. *Adv. Drug Delivery Rev.* **2002**, *54*, 453−456.

(39) Lutz, J.-F. Polymerization of oligo(ethylene glycol) (meth)-acrylates: Toward new generations of smart biocompatible materials. *J. Polym. Sci., Part A: Polym. Chem.* **2008**, *46*, 3459−3470.

(40) Kopeček, J.; Kopečková, P. HPMA copolymers: Origins, early developments, present, and future. *Adv. Drug Delivery Rev.* **2010**, *62*, 122−149.

(41) Debayle, M.; Balloul, E.; Dembele, F.; Xu, X.; Hanafi, M.; Ribot, F.; Monzel, C.; Coppey, M.; Fragola, A.; Dahan, M.; Pons, T.; Lequeux, N. Zwitterionic polymer ligands: an ideal surface coating to totally suppress protein-nanoparticle corona formation? *Biomaterials* **2019**, *219*, 119357.

(42) García, K. P.; Zarschler, K.; Barbaro, L.; Barreto, J. A.; O'Malley, W.; Spiccia, L.; Stephan, H.; Graham, B. Zwitterionic-Coated "Stealth" Nanoparticles for Biomedical Applications: Recent Advances in Countering Biomolecular Corona Formation and Uptake by the Mononuclear Phagocyte System. *Small* **2014**, *10*, 2516−2529.

(43) Nicolas, J. Drug-Initiated Synthesis of Polymer Prodrugs: Combining Simplicity and Efficacy in Drug Delivery. *Chem. Mater.* **2016**, *28*, 1591−1606.

(44) Harrisson, S.; Nicolas, J.; Maksimenko, A.; Bui, D. T.; Mougin, J.; Couvreur, P. Nanoparticles with In Vivo Anticancer Activity from Polymer Prodrug Amphiphiles Prepared by Living Radical Polymerization. *Angew. Chem., Int. Ed.* **2013**, *52*, 1678−1682.

(45) Bao, Y.; Boissenot, T.; Guégain, E.; Desmaële, D.; Mura, S.; Couvreur, P.; Nicolas, J. Simple Synthesis of Cladribine-Based Anticancer Polymer Prodrug Nanoparticles with Tunable Drug Delivery Properties. *Chem. Mater.* **2016**, *28*, 6266−6275.

(46) Guégain, E.; Tran, J.; Deguettes, Q.; Nicolas, J. Degradable polymer prodrugs with adjustable activity from drug-initiated radical ring-opening copolymerization. *Chem. Sci.* **2018**, *9*, 8291−8306.

(47) Louage, B.; Nuhn, L.; Risseeuw, M. D. P.; Vanparijs, N.; De Coen, R.; Karalic, I.; Van Calenbergh, S.; De Geest, B. G. Well-Defined Polymer−Paclitaxel Prodrugs by a Grafting-from-Drug Approach. *Angew. Chem., Int. Ed.* **2016**, *55*, 11791−11796.

(48) Di Consiglio, E.; Darney, K.; Buratti, F. M.; Turco, L.; Vichi, S.; Testai, E.; Lautz, L. S.; Dorne, J. L. C. M. Human Variability in Carboxylesterases and carboxylesterase-related Uncertainty Factors for Chemical Risk Assessment. *Toxicol. Lett.* **2021**, *350*, 162−170.

(49) Li, D. The Impact of Carboxylesterases in Drug Metabolism and Pharmacokinetics. *Curr. Drug Metab.* **2019**, *20*, 91−102.

(50) Bao, Y.; De Keersmaecker, H.; Corneillie, S.; Yu, F.; Mizuno, H.; Zhang, G.; Hofkens, J.; Mendrek, B.; Kowalczuk, A.; Smet, M. Tunable Ratiometric Fluorescence Sensing of Intracellular pH by Aggregation-Induced Emission-Active Hyperbranched Polymer Nanoparticles. *Chem. Mater.* **2015**, *27*, 3450−3455.

(51) D'Souza, A. J. M.; Topp, E. M. Release from polymeric prodrugs: Linkages and their degradation. *J. Pharm. Sci.* **2004**, *93*, 1962−1979.

(52) Ragelle, H.; Danhier, F.; Préat, V.; Langer, R.; Anderson, D. G. Nanoparticle-based drug delivery systems: a commercial and regulatory outlook as the field matures. *Expert Opin. Drug Delivery* **2017**, *14*, 851−864.

(53) Joint FAO/WHO Consultation on Health Implications of Acrylamide in Food (2002 : Geneva, Switzerland) & WHO Food Safety Programme. (2002). *Health implications of acrylamide in food : report of a joint* FAO/WHO consultation, WHO Headquarters, Geneva, Switzerland, 25−27 June 2002. World Health Organization

(54) Andersen, F. A. Amended Final Report on the Safety Assessment of Polyacrylamide and Acrylamide Residues in Cosmetics. *Int. J. Toxicol.* **2005**, *24*, 21−50.

(55) Watt, R. P.; Khatri, H.; Dibble, A. R. G. Injectability as a function of viscosity and dosing materials for subcutaneous administration. *Int. J. Pharm.* **2019**, *554*, 376−386.

(56) Royer, I.; Alvinerie, P.; Wright, M.; Monsarrat, B.; Ho, L. K.; Armand, J. P. Paclitaxel metabolites in human plasma and urine: Identification of 6α-hydroxytaxol, 7-epitaxol and taxol hydrolysis products using liquid chromatography/atmospheric-pressure chemical ionization mass spectrometry. *Rapid Commun. Mass Spectrom.* **1995**, *9*, 495−502.

(57) Volk, K. J.; Hill, S. E.; Kerns, E. H.; Lee, M. S. Profiling degradants of paclitaxel using liquid chromatography−mass spectrometry and liquid chromatography−tandem mass spectrometry substructural techniques. *J. Chromatogr., B* **1997**, *696*, 99−115.

(58) Rowinsky, E. K.; Donehower, R. C. The clinical pharmacology of paclitaxel (Taxol). *Semin. Oncol.* **1993**, *20*, 16−25.

(59) Dorr, R. T.; Snead, K.; Liddil, J. D. Skin ulceration potential of paclitaxel in a mouse skin model in vivo. *Cancer* **1996**, *78*, 152−156.

(60) Shin, B. S.; Kim, H. J.; Hong, S. H.; Lee, J. B.; Hwang, S. W.; Lee, M. H.; Yoo, S. D. Enhanced absorption and tissue distribution of paclitaxel following oral administration of DHP 107, a novel mucoadhesive lipid dosage form. *Cancer Chemother. Pharmacol.* **2009**, *64*, 87−94.

(61) Marupudi, N. I.; Han, J. E.; Li, K. W.; Renard, V. M.; Tyler, B. M.; Brem, H. Paclitaxel: a review of adverse toxicities and novel delivery strategies. *Expert Opin. Drug Saf.* **2007**, *6*, 609−621.

(62) Nieto, Y.; Cagnoni, P. J.; Bearman, S. I.; Shpall, E. J.; Matthes, S.; DeBoom, T.; Barón, A.; Jones, R. B. Acute encephalopathy: a new toxicity associated with high-dose paclitaxel. *Clin. Cancer Res.* **1999**, *5*, 501−506.

(63) Zhu, A. Z. Quantitative translational modeling to facilitate preclinical to clinical efficacy & toxicity translation in oncology. *Future Sci. OA* **2018**, *4*, FSO306.